Modeling the seasonal and interannual variability (2001-2010) of chlorophyll-a in the Iberian margin

Rosa Reboreda[a,1,*], Nuno G. F. Cordeiro[a], Rita Nolasco[a], Carmen G. Castro[b], Xosé A. Álvarez-Salgado[b], Henrique Queiroga[c], Jesus Dubert[a]

[a] *CESAM and Departamento de Física, Universidade de Aveiro, Campus de Santiago, 3810-194, Aveiro, Portugal*
[b] *IIM-CSIC, Instituto de Investigacións Mariñas, Eduardo Cabello 6, 36208 Vigo, Spain*
[c] *CESAM and Departamento de Biologia, Universidade de Aveiro, Campus de Santiago, 3810-194, Aveiro, Portugal*

Abstract

A modeling study of the seasonal and interannual variability of chlorophyll-a has been carried out for the period 2001-2010 along the Iberian shelf and adjacent ocean. A high resolution regional configuration of the three-dimensional Regional Ocean Modeling System (ROMS) has been used, coupled to a N_2PZD_2-type biogeochemical model. Chlorophyll-a concentration ([Chl]) model outputs were compared to regional objective analysis of remotely sensed [Chl] data for the same period. The spatio-temporal variability of modeled and satellite derived [Chl] was analyzed applying an individual Empirical Orthogonal Function (EOF) analysis to monthly time series. Three main modes of sea surface [Chl] variability explained more than 90% of modeled variability and more than 85% of remotely sensed variability. The first EOF accounted for the spring phytoplankton bloom (March-April). The second EOF was related to the spring-summer coastal upwelling season (April-September). The third EOF showed a recurrent [Chl] minimum in winter coinciding with the maximum vertical mixing (February) for the northern part of the region. The influence of the hydrographic conditions on

*Corresponding author
Email addresses: rosa.reboreda@ua.pt (Rosa Reboreda), ngfc@ua.pt (Nuno G. F. Cordeiro), rita.nolasco@ua.pt (Rita Nolasco), cgcastro@iim.csic.es (Carmen G. Castro), xsalgado@iim.csic.es (Xosé A. Álvarez-Salgado), henrique.queiroga@ua.pt (Henrique Queiroga), jdubert@ua.pt (Jesus Dubert)
[1] Tel: +351 234 378 100

[Chl] variability was explored through a cross-correlation analysis of the three EOFs and an assortment of physical descriptors given by the model: namely the mixing/stratification cycles and the occurrence of coastal upwelling.

Keywords: chlorophyll, upwelling, spring bloom, modeling, North East Atlantic, Iberian margin

1. Introduction

The coastal ocean supports 80-90% of the global new production due to the enhanced land-ocean-atmosphere interaction that occur in these regions (Chen et al., 2003). Nutrient rich continental and atmospheric inputs, and the hydrodynamics resulting from the interaction of the coastal currents with bathymetry, coastal morphology and the atmospheric-ocean interaction strongly influence the primary production through a tight physical-biogeochemical coupling. The high spatio-temporal variability in some of these factors result in large chlorophyll-a variability (proxy of phytoplankton biomass and primary production) at event, seasonal and interannual time scales.

The seasonal pattern of chlorophyll in the Iberian margin (Fig. 1) is characterized by high concentrations from May to September, when northeasterly winds prevail along the N-S oriented Western Iberian coast. These winds induce the upwelling of cold and nutrient rich Eastern North Atlantic Central Water (ENACW) in intermittent pulses (Fraga, 1981; Peliz et al., 2002; Relvas et al., 2007). By the end of summer (September-October), there is a shift in the wind regime to downwelling favorable southwesterlies, along with the onset of the relatively warm and saline Iberian Poleward Current (IPC) over the slope (Haynes and Barton, 1990; Peliz et al., 2005; Relvas et al., 2007). This change of regime is usually associated to a phytoplankton autumn bloom in the coast (Castro et al., 1997; Álvarez-Salgado et al., 2003; Silva et al., 2009), followed by a decrease in chlorophyll concentration ([Chl]) in winter. Nonetheless, episodic uwpelling events during winter can increase [Chl]. Furthermore, the presence of the Western Iberia Buoyant Plume (WIBP; Peliz et al., 2002), a low-salinity water lens originated by accumulated river runoff, supplies stratification conditions suitable for phytoplakton growth (Ribeiro et al., 2005). From interannual observations (1984-1992) in the N-NW Iberian shelf, Bode et al. (1996) obtained that average [Chl] during bloom stages (upwelling/spring/autumn blooms) were double of the concentrations in periods of thermal stratification (summer), which in turn were about twice the concentrations during winter.

This general seasonal variability presents, however, noticeable interannual differences in the timing (month) of maximum offshore and shelf primary production (Joint et al., 2002), in new production associated to upwelling (Álvarez-Salgado et al., 2002), or in the onset and cessation of the downwelling period (Álvarez-Salgado et al., 2003). It is generally accepted that the interannual and seasonal variability in physical forcings leads to these changes in biological production or, as described in Silva et al. (2009), to shifts in the phytoplankton community structure. Other sources of variability, independent of physical forcing may occur as a result of complex, non-linear interactions in the ecosystem (Williams and Follows, 2003). Also, a positive interannual trend in primary production has been detected (13.71 mg C m^{-2} d^{-1} yr^{-1})(Bode et al., 2011). Understanding the physical-biogeochemical interactions that may underly the variability in [Chl] would help to elucidate the ecosystem variability, intimately related to the rich marine biodiversity and fishing resources of the region (Tenore et al., 1995; Figueiras et al., 2002; Santos et al., 2005).

Inherent difficulties exist to obtain high quality long-term observations of physical and particularly biogeochemical variables, specially for a large region like this. Thus, despite the efforts made to implement monitoring programmes (e.g. Otero et al., 2011), long-term time series are yet not available. This makes difficult a robust statistic analysis to characterize the seasonal and interannual variability. The current knowledge is mostly based on observations unequally distributed in time and space. Ocean numerical models can help to overcome this gap, by complementing observations and allowing to explore the physical-biogeochemical interactions through coupled hydrodynamic-biogeochemical models (Machu et al., 2005; Gruber et al., 2006; Echevin et al., 2008). The Regional Ocean Modeling System (ROMS) has contributed to the understanding of the ocean dynamics and hydrography in Western Iberia (e.g. Peliz et al., 2007, 2009; Nolasco et al., 2013), including some ecosystem applications (Oliveira et al., 2009). In this study a high resolution regional configuration of ROMS coupled to a NPZD-type (Nutrients-Phytoplankton-Zooplankton-Detritus) biogeochemical model has been implemented to the Iberian margin for the decade 2001-2010. The aim was to reproduce the interannual variability in [Chl] over this period, study the main modes of [Chl] variability and correlate this variability with the hydrographic conditions. The studied period allows an analysis of the current variability, establishing a reference when studying changes in the future. The [Chl] and Sea Surface Temperature (SST) obtained from model results were evaluated comparing time series of modeled [Chl] and SST with satellite observations for the same period. In order to identify the main modes of [Chl] variability an Empirical Orthogonal Function (EOF) analysis of modeled and satellite [Chl] time series (domain averaged) was carried out. Then, we correlate the main modes of [Chl] variability with an assortment of physical forcings using model data. The aim was to elucidate some mechanisms of physical-biogeochemical coupling that may underlay the ecosystem functioning and variability. The [Chl] variability in the water column was also explored, firstly comparing model outputs to weekly observations at a shelf station along one year (May 2001-April 2002), and then extending the [Chl] variability over the 10 years for that location using model results.

2. Methods

2.1. Model setup

2.1.1. Hydrodynamic model

The interannual simulation of the period 2001-2010 was run for a high resolution regional configuration of the Regional Ocean Modeling System (ROMS) (Shchepetkin and McWilliams, 2005; Haidvogel et al., 2008; Penven et al., 2006) for the Iberian margin. ROMS is a three dimensional (3D) ocean circulation model with free-surface, vertical terrain-following coordinates (sigma-coordinates), and horizontal orthogonal curvilinear coordinates, designed to resolve regional problems, such as coastal areas and regional seas at the mesoscale. A two-domain approach was used, as shown in Figure 1: A large-scale or first domain (FD) was run independently (offline) in order to provide initial and boundary conditions to our second domain (SD). The FD included the northeast Atlantic region between 30° N - 48° N and 0.8° E - 32° W, and had 1/10°($\sim$9 km) horizontal resolution and 30 vertical s-levels, in order to resolve the large-scale circulation features. The second domain (SD) included the western Iberia from the Gulf of Cádiz to Galicia (34.5° N - 45.5° N and 5.5° W - 12.5° W; $\sim$1200 x 600 km) (Fig. 1). It had horizontal resolution of 1/27°($\sim$3 km) and 60 vertical s-levels in order to properly resolve the Mediterranean undercurrent, whose circulation is known to influence the surface transport of chemical and biological properties (Serra et al., 2010). A more detailed description of this regional configuration of ROMS can be found in Nolasco et al. (2013).

A climatological run of the 5th year of the FD (Nolasco et al., 2013) was used as the initial state to run a realistic simulation of the hydrodynamic model for the period 2001-2010 for this outer domain. The surface forcing was extracted from NCEP 2 reanalysis for air-sea fluxes (2001-2010), provided by the NOAA (http://www.esrl.noaa.gov/psd/) and QuikSCAT surface wind reanalysis (2001–2008) at 0.5° × 0.5° spatial resolution provided by CERSAT (http://www.ifremer.fr/cersat). For 2009 and 2010, ASCAT surface wind reanalysis (0.25° × 0.25° spatial resolution) was used, also provided by CERSAT, since QuikSCAT mission stopped towards the end of 2009 (Fig. 2 upper panel). For the SD, the year 2001 was initialized from 1st January using initial conditions from a previous climatological run of the coupled hydrodynamic-biogeochemical model (9th year) for this domain (Reboreda et al., in revision). The physical boundary conditions were provided by the simulation of 2001–2010 for the FD, and the same surface forcing was applied. The exchange of Atlantic and Mediterranean waters at the Strait of Gibraltar was explicitly represented in the SD by the imposition of vertical profiles of temperature, salinity and zonal velocity at 5 grid points at the Strait, similarly to Peliz et al. (2007).

The freshwater continental runoff from the main rivers of the region was included with realistic discharge values for 2001-2010 provided by Instituto Nacional da Água (INAG; http//inag.pt) when available (Fig. 2 lower panel). When no realistic discharges were available, climatological values were obtained from INAG for the Portuguese rivers, and from Río-Barja and Rodríguez-Lestegás (1992) for the Galician rivers.

2.1.2. Biogeochemical model

A biogeochemical model was run coupled to the hydrodynamic model to simulate the base trophic levels and biogeochemical components of the system. The $N_2ChlPZD_2$ model consists of a nitrogen based model, computing 7 state variables: two nutrient compartments, nitrate (NO_3) and ammonium (NH_4), phytoplankton ($Phyt$), zooplankton (Zoo), and two detritus compartents, fast-sinking large detritus ($LDet$) and slow-sinking small detritus ($SDet$), all expressed in mmol N m^{-3} (Fig. 3). Additionally, chlorophyll-a (mg m^{-3}) is derived from phytoplankton concentration using a variable chlorophyll:carbon ratio, θ (mg chlorophyll-a (mg C)$^{-1}$) and a constant C:N Redfield ratio of 6.625 (mmol C (mmol N)$^{-1}$). The variable θ describes the proportion of photosynthetically fixed carbon that is used for chlorophyll-a biosynthesis considering the model of Geider et al. (1997). Its implementation in the ROMS biogeochemical model is described in Gruber et al. (2006) (online additional material).

The 3D time evolution of any of the biogeochemical variables (B_i) is calculated considering its diffusion, horizontal advection, vertical mixing and the biogeochemical processes that act as sink or source for the variable:

$$\frac{\partial B_i}{\partial t} = \nabla \cdot K \nabla B_i - u \cdot \nabla_h B_i - (w + w_{sink}) \frac{\partial B_i}{\partial z} + SMS(B_i) \tag{1}$$

where K is the eddy kinematic diffusivity tensor, u is the horizontal velocity, w and w_{sink} are the vertical velocity and the vertical sinking rate of the biogeochemical variable (all particulated variables, except zooplankon), respectively. The biogeochemical processes included in the source minus sink (SMS) term are specific for each variable.

The following set of SMS equations for each of the biogeochemical variables was used.

$$SMS(NO_3) = -\mu(PAR, T) \cdot \mu(NO_3) \cdot Phyt + t_{NH4_{nitr}}\ NH_4 \tag{2}$$

$$\begin{aligned} SMS(NH_4) = {} & -\mu(PAR, T) \cdot \mu(NH_4) \cdot Phyt - t_{NH4_{nitr}}\ NH_4 + t_{Z_{metab}}\ Zoo \\ & + t_{SD_{remin}}\ SDet + t_{LD_{remin}}\ LDet \end{aligned} \tag{3}$$

$$\begin{aligned} SMS(Phyt) = {} & \mu(PAR, T) \cdot \mu(NO_3, NH_4) \cdot Phyt - m_{PD}\ Phyt \\ & - g_{max}\ Zoo\ \frac{Phyt}{K_P + Phyt} \end{aligned} \tag{4}$$

$$SMS(Zoo) = \beta\ g_{max}\ Zoo\ \frac{Phyt}{K_P + Phyt} - m_{ZD}\ Zoo - t_{Z_{metab}}\ Zoo \tag{5}$$

$$\begin{aligned} SMS(SDet) = {} & m_{PD}\ Phyt + m_{ZD}\ Zoo + (1 - \beta)\ g_{max}\ Zoo\ \frac{Phyt}{K_P + Phyt} \\ & - t_{SD_{remin}}\ SDet - S_{agg}\ SDet \cdot (Phyt + SDet) \end{aligned} \tag{6}$$

$$SMS(LDet) = -t_{LD_{remin}}\ LDet + Sagg \cdot (Phyt + SDet)^2 \tag{7}$$

$$SMS(\theta) = \mu(PAR, T) \cdot \mu(NO_3, NH_4) \cdot \left(\frac{\mu(T) \cdot \mu(NO_3, NH_4) \cdot \theta_{max}}{\sqrt{\mu(T)^2 + (\alpha\ PAR\ \theta)^2}} - \theta \right) \tag{8}$$

The biogeochemical processes and formulations included in the SMS equations are mostly the same described in Gruber et al. (2006), although some formultations are from Koné et al. (2005) (see Table 1). Model parameters values for the sink/source terms selected to represent our region of study with this model are listed in Table 2. These parameters aimed at representing the eutrophic coastal ecosystem and the offshore spring bloom, both dominated by diatoms. This necessarily implied reducing the ability of the model to correctly represent the oligotrophic offshore environment, dominated by nanophytoplankton, as only one phytoplankton functional group was included.

The NO_3, $Phyt$ (and chlorophyll-a), and Zoo for the model initial conditions (January 2001) were obtained from the 9th year of a climatological simulation of a simpler $NChlPZD$ biogeochemical model (Reboreda et al., in revision). Boundary conditions for NO_3 and chlorophyll-a were taken from the climatological data sets of the World Ocean Atlas 2009 (Garcia et al., 2010) and SeaWiFS, respectively. For NO_3, seasonal (for depths down to 500 m) and annual (depths below 500 m) climatologies were used. For chlorophyll-a, the seasonal climatology of surface concentrations from SeaWiFs data was used. Seasonal vertical profiles were created from these surface concentrations using the algorithm of Morel and Berthon (1989). Boundary values of $Phyt$ and Zoo were derived from chlorophyll-a ($Phyt = 0.5 \cdot Chl$; $Zoo = 0.2 \cdot Chl$), as in Gruber et al. (2006). Boundary conditions were supplied seasonally. NH_4, $SDet$, and $LDet$ initial and boundary conditions were not available from climatological data sets, so they were introduced as constant analytical values: 0.1 mmol N m^{-3} (NH_4) and 0.02 mmol N m^{-3} (both detritus sizes). Constant riverine inputs of NO_3 and chlorophyll-a were used along the year, with the values indicated in Marta-Almeida et al. (2012).

2.2. Data series for model evaluation

Model sea surface temperature (SST) and [Chl] outputs were evaluated by comparison with satellite products for the period 2001-2010. Daily SST was compared with data retrieved from the Advanced Very High Resolution Radiometer (AVHRR) of the National Oceanic and Atmospheric Administration (NOAA). The data were extracted from the EUMETSAT Ocean & Sea Ice Satellite Application Facility (OSI-SAF) (www.osi-saf.org) and made available by CERSAT (IFREMER, France). The product has an approximate horizontal resolution of 2 km. Daily surface [Chl] was compared with CERSAT-IFREMER ocean color derived (OC5 algorithm) [Chl] obtained from merging the following three sensors: Sea-viewing Wide Field of View Sensor (SeaWiFS) on the Orbview platform (January 01, 1998-December 31, 2004), Moderate Resolution Imaging Spectroradiometer (MODIS) on the Aqua platform (October 01, 2002 to present), and the MEdium Resolution Imaging Spectrometer Instrument (MERIS) on the ENVISAT platform (October 01, 2002–April 08, 2012) (ftp://ftp.ifremer.fr/ifremer/cersat/products/gridded/ocean-color/atlantic/EUR-L4-CHL-ATL-v01/). The optimal interpolation merging method, which provides cloudless daily fields of [Chl], was described and validated in Saulquin et al. (2011). The product is provided at 1.1 km horizontal resolution.

Model outputs were also compared with in situ observations obtained at a 1-year intensively sampled shelf station off the Galician coast (NW Iberian margin, Fig. 1). The station was weekly sampled between 15th May 2001 and 24th April 2002 within the frame of the DYBAGA project. A detailed description of the hydrography of this site over that period can be found in Nieto-Cid et al. (2004), Álvarez-Salgado et al. (2006), and Herrera et al. (2008). The corresponding succession of microplankton has been described in Espinoza-González et al. (2012).

Additionally, a mixed layer depth (MLD) monthly climatology (2002-2010) constructed from ARGO floats profiles (Holte and Talley, 2009; Holte et al., 2010) was used to evaluate the MLD derived from model outputs. These authors calculated the MLD using a hybrid algorithm between the classical threshold method and the shape of the profile for either potential density, potential temperature, or salinity profiles. MLD calculated with the temperature algorithm were used to compare with our modeled MLD. Our method for calculating the MLD considered a 0.2 °C temperature threshold relative to a surface reference level of 10 m, in order to avoid the effect of surface diurnal heating (de Boyer Montégut et al., 2004), establishing a maximum MLD of 450 m. Given that some of the years in the Holte et al. (2010) dataset had few values within the area of the model domain, and/or they were unevenly distributed, we selected only the years having more than 200 MLD values and presenting an homogeneous distribution within the model domain (2005-2008). Then, an spatial MLD mean was calculated for each of these years.

2.3. Statistical analysis

2.3.1. Model error statistics

Model error relative to satellite observations of surface [Chl] were calculated applying four reliability indices commonly used for ocean-ecosystem models validation (Allen et al., 2007; Stow et al., 2009; Warner et al., 2005). They were calculated on a daily basis. The indices are briefly described next, with an explanation of the type of information they provide about the model performance:

Bias gives an indication of whether the model is systematically overestimating or underestimating the observations. The closer the bias is to zero, the better the model.

$$Bias = \frac{\sum_{n=1}^{n}(M_n - D_n)}{\sum_{n=1}^{n} D_n} \tag{9}$$

where M is the model estimation, D the data, and n is the number of comparisons of total grid points.

Rms is the *root mean squared error* of n model-data comparisons (total grid points).

$$rms = \sqrt{\frac{\sum_{n=1}^{n}(M_n - D_n)^2}{n}} \tag{10}$$

The closer the rms to zero the better the fit between the model and observations.

Skew gives the degree of asymmetry of the error distribution.

$$Skew = \frac{N}{(N-1)(N-2)} \sum_{n=1}^{n} \left(\frac{(M_n - D_n) - (\overline{M_n - D_n})}{\sigma_D} \right)^3 \tag{11}$$

where N is the total number of model-data matches, and σ_D the standard deviation of the data. Positive skewness indicates that model tends to make more overestimations, whereas negative skewness indicates that model tends to make more underestimations.

Skill is a measure of the quantitative agreement between the model and observations where M_n is compared with a time mean $\overline{D}$.

$$Skill = 1 - \frac{\sum |M_n - D_n|^2}{\sum(|M_n - \overline{D}| + |D_n - \overline{D}|)^2} \tag{12}$$

Perfect agreement between model results and observations would yield a skill of one, and complete disagreement would correspond to zero model skill.

2.3.2. Empirical Orthogonal function analysis

The spatio-temporal variability of modeled and satellite derived [Chl] was analyzed applying an individual Empirical Orthogonal Function (EOF) analysis to monthly time series. The EOF analysis consists of a representation of the data in terms of a reduced set of orthogonal functions or modes (Glover et al., 2011). The outputs consist of spatial fields and their associated relative variance (eigenvalues) and temporal weightings (eigenvectors), allowing to study the temporal and spatial variability of data (Shutler et al., 2011). For that, we created an $N \times M$ data matrix X, consisting of N time data and M grid points, i.e., a 10 year record of monthly averages ($N = 120$) of [Chl] on a grid of $M = 320 \times 162$ points. This grid was smaller than the actual model grid (390×189 points) because half degree was removed from each boundary of the model domain to avoid using points near the boundaries, where climatological [Chl] values (SeaWiFS) were applied when running the model. The M grid of satellite data had the same number of points used for the model ($M = 320 \times 162$), as an interpolation of the original grid to the model grid was performed and the same boundary points were removed. The EOF eigenvectors and eigenvalues were obtained via singular value decomposition (SVD) of X (Preisendorfer, 1988) as $X = BL^{1/2}F^T$, where L is the diagonal matrix of the eigenvalues giving information on the percentage variance explained in each EOF, F is the right matrix of eigenvectors (the spatial field), and B is the left matrix of eigenvectors which is used to obtain the temporal mode (temporal mode $= B \times L$). Three EOFs were retained for analysis.

2.3.3. Cross-correlation analysis

The possible physical forcings underlying the three [Chl] EOFs with the largest eigenvalues were explored by performing an individual cross-correlation analysis between each of the modeled EOFs time series and the corresponding time series of the physical forcing to be tested. All correlations presented have a 95% confidence interval. The cross-correlation analysis was selected because it would allow to find not only the degree of correspondence between the two time series, but also the possible time lags between them. Thus, a significant correlation may imply a causality between the physical forcing and the biological response, although bearing in mind that it does not proof it, as a co-causal relationship may also exist (Glover et al., 2011).

The spatial correlations between each of the three [Chl] temporal EOFs and the physical forcings (at each grid point) were also explored. This analysis was carried out only for the physical forcings that showed the maximum correlation with each EOF in the cross-correlation analysis of the domain averaged time series (with the corresponding time lag).

3. Results and discussion

3.1. Model evaluation: temporal series of [Chl] and SST

Sea surface [Chl] time series averaged over the study region showed a conspicuous peak detected every year, corresponding to the North Atlantic spring bloom (March-April) (Fig. 4a). The model reproduced the spring bloom captured by the satellite observations, although it occurred earlier and with [Chl] values generally higher than observed. This difference was highly variable from year to year (0.5-2 mg m^{-3}). The best correspondence occurred for year 2009, when both peaks (modeled and observed) were nearly coincident. The model also satisfactorily reproduced the seasonal evolution of the domain averaged SST (Fig. 4c), showing the characteristic succession of winter minima and summer maxima, with similar values to observations. Over the shelf, the model was able to reproduce the high [Chl] variability with concentration values close to observations (Fig. 4b). From April to September recurrent [Chl] maxima over the shelf, associated to the upwelling of cold and nutrient rich subsurface waters, were captured by the model (Figs. 4b and d). Exceptionally, years 2009 and 2010 were not well reproduced by the model in terms of [Chl], with model values being systematically lower than observations. On the other hand, modeled SST during the upwelling season seemed to improve for these two years, as temperature minima were more close to satellite observation than in previous years, when SST reached noticeably lower minima in the model (Fig. 4d). We have evidences that these changes in 2009 and 2010 were related to the shift from QuikSCAT to ASCAT wind products for the surface model forcing. The use of ASCAT seemed to improve the model results related to the upwelling reducing its intensity, probably due to the higher spatial resolution of wind stress compared to QuikSCAT. The latter tends to overestimate alongshore winds due to its limitations representing the coastal wind drop-off (Albert et al., 2010). Accordingly, a possible reduction in the modeled upwelling intensity would lead to: (1) an increase in modeled SST and (2) a reduction of the modeled nitrate input and thus less [Chl] over the shelf.

Table 3 presents statistics that quantify the model ability to reproduce the observed (satellite derived) [Chl] interannual variability for the period 2001-2010. All the indices showed a considerable variability among years, which indicated that model-satellite differences were not constant. Still, general trends for model-satellite comparisons could be distinguished. Regardless of the mentioned overestimation in modeled [Chl] during the spring bloom (Fig. 4a), the model bias and skew indicated that the model tended to slightly underestimate surface [Chl] for most part of the year (negative values in Table 3). Underestimation was particularly detected in the years 2009 and 2010, coinciding with the shifts already discussed for the shelf. However, it should be noted that the years 2009 and 2010 still had a good skill, because of the good model-satellite match on the spring bloom. On the other hand, the year 2005 stand out for the highest positive bias, skew and rms, as expected for the strong spring bloom simulated (Fig. 4a). Model skill pointed to 2009, 2004, and 2003 as the years of best model-satellite correspondence, whereas 2006, 2007, and 2005 as years of worst correspondence.

It should be considered that some uncertainties are also associated to the satellite observations (Gregg and Casey, 2007). These can be originated by errors in the algorithm estimations of [Chl], as the overestimations reported in the coastal zone when using SeaWiFS data (Le Fouest et al., 2006). In the shelf region of the Iberian Peninsula, [Chl] overestimations have also been reported when using MERIS and MODIS data (case 1 waters) (Oliveira et al., 2007). On the other hand, underestimations were detected during the validation of the method used for merging SeaWiFS/MODIS/MERIS data (dataset used here) with in situ data in the west French coast (Saulquin et al., 2011).

3.2. Main modes of [Chl] variability: EOF analysis of model and satellite observations

An EOF analysis was carried out to split the modeled and remotely sensed [Chl] variability into statistical modes that would give an initial idea of the processes that contribute for that variability. Also, comparing the EOF analysis of model outputs and observations would let us evaluate to what extent was the model able to reproduce the observed variability. Three [Chl] EOFs were retained for analysis, which explained more than 90% of modeled variability and more than 85% of remotely sensed variability. For each EOF, the spatial variability (spatial field) and its associated time series of amplitude (temporal mode) are presented (Figs. 5,6,7). The contribution of one EOF at any time in a particular point is obtained by multiplying the value at that location times the value of the temporal coefficient at a given time.

The first mode of the EOF analysis of [Chl] explained 69.25% of [Chl] variability in the model and 46.32% of variability in the remotely sensed [Chl] (Fig. 5). The latter percentage was coincident with the first EOF mode found by Miles and He (2010) (46.35%) when analyzing satellite (MODIS) [Chl] data for the South Atlantic Bight over 2003-2008. The temporal evolution showed that this mode captures the seasonality of the spring bloom (March-April) in both model results and observations, which followed the seasonal solar heating cycle of the water column, reflected in the MLD seasonality (Fig. 8). The maximum model MLD generally occurred in February (winter mixing), which was confirmed by the MLD obtained from ARGO floats, and followed by the spring thermal stratification in March-April (Fig. 8), coinciding with the increase in [Chl] detected in the temporal mode of the EOF 1 (Fig. 5). The comparison of the MLD derived from model results and ARGO profiles showed that the mean winter mixing over the domain tended to be deeper in the observations than in the model, in particular for years of deepest MLD (Fig. 8). The EOF 1 (Fig. 5) confirmed the trend for the anticipation ($\sim$1 month) of the spring bloom in the model mentioned in section 3.1. The same anticipation was generally detected on the spring shoaling of the MLD in the model, with MLD values in March usually shallower in the model than observed. This happened because the shoaling started from a shallower winter mixing (Fig. 8). Thus, the shallower MLD in March was the possible reason for the bloom anticipation. The spatial field of model EOF 1 indicated that this variability affected mainly the offshore region, with a noticeable latitudinal gradient from higher [Chl] in the north to lower values in the south during the bloom. This latitudinal gradient was also evident in the satellite EOF 1, although the latter showed also a clear zonal component, with increasing [Chl] towards the shelf, which was absent in the model EOF 1 (Fig. 5). Considering this discrepancy between the model and the satellite spatial field, it should be considered that the timing of the bloom (March-April) is coincident with the maximum river outflow in the region. Thus, high concentration of suspended matter from river outflow may interfere with remotely sensed [Chl], resulting in a overestimation. On the other hand, the lack of seasonal varying nitrate concentration from continental inputs in the model may be a limitation over the shelf, leading to a misrepresentation of nutrient inputs. The temporal mode of the satellite EOF 1 also revealed a smaller peak which occurred between August and November, i.e., late summer or autumn. The peak was not present in the temporal mode of the model EOF (Fig. 5). The timing of the signal would suggest the increase in [Chl] associated with the autumn bloom (Castro et al., 1997; Álvarez-Salgado et al., 2003; Silva et al., 2009). However, this peak in the satellite temporal mode had frequently a negative or nearly zero value, which multiplied by the positive value of the spatial field would actually indicate a negligible effect increasing [Chl]. The difference in the percentages explained by the model and by the satellite observations in EOF 1 indicated that the seasonal variability associated to the spring bloom dominated the variability in model outputs, whereas, still being the most important, it was lower in satellite data.

The second EOF explained 14.45% of modeled vs. 26.54% of observed [Chl] variability (Fig. 6). The temporal and spatial fields together indicated that this variability accounted for the increase in [Chl] during the spring-summer upwelling season (April-September) over the shelf. The increase in [Chl] is driven by the upwelling of subsurface cold and nutrient rich ENACW under prevailing northerly winds along the Iberian margin (Fig 2, upper panel). The [Chl] was higher in the model than in observations, and affected a larger shelf area, extending to the southwestern shelf (Fig. 6). The temporal mode showed a variable intensity of the spring-summer upwelling signal from year to year, as expected from the known variable intensity and persistence of the northerly winds (e.g. Álvarez-Salgado et al., 2002). For example, years of strong and persistent northerly winds, such as 2001, 2002, and 2006 (Fig 2) were also years with a noticeable [Chl] signal of the temporal EOF 2 (Fig. 6). Years of more variable winds, such as 2003 and 2004 (Fig 2) presented an intermittent [Chl] signal of the temporal EOF 2 over the upwelling season (Fig. 6). Sánchez et al. (2007) showed that this strengthening and weakening of upwelling-favorable northerlies had a significant relationship with the North Atlantic Oscilation (NAO) phases (interplay between the Azores High-Iceland Low). The spatial field of EOF 2 also revealed a slight decrease of the offshore [Chl] in summer, reflecting the nutrient depletion due to thermal stratification.

The third EOF mode explained 9.67% of modeled [Chl] variability and 13.42% of the observed variability (Fig. 7). The temporal and spatial analysis pointed out to a decrease (increase) in [Chl] in winter (spring) in the northern offshore region of the domain, both in model outputs and observations. A similar pattern also affected the shelf, in particular the innermost part. There was an opposite pattern in the offshore region south of ∼43° N, i.e., a progressive increase in [Chl] in winter and a subsequent decrease after February-March. This variability suggested it might be associated to the cycle of winter vertical mixing, which is maximum in February for the Iberian region as already mentioned (Fig. 8). It would tend to decrease [Chl] north of ∼43° N by a dilution/light limitation effect also known as a *phyto-convection* mechanism, proposed for several oceanic regions and also described for the NW Iberia oceanic region in Perez et al. (2005). The late winter (February-March) MLD in the Iberian margin reaches 150 m south of 43° N, and more than 300 m to the north (Arhan et al., 1994; Álvarez-Salgado et al., 2003), which is coincident with the latitudinal limit found in the spatial field of EOF 3. South of that latitude, the deepening of the MLD throughout winter seemed to favor [Chl] increase, providing new nutrients to the surface after the summer depletion. These opposite mechanisms were also proposed by Follows and Dutkiewicz (2001) to explain the bloom evolution in the subtropical and subpolar North Atlantic. The negative peak of this winter signal in the model EOF 3 (February) tended to precede in 1 month the peak on the satellite EOF 3 (March) (Fig. 7, upper panel). Thus, in the model, the winter [Chl] minimum in the North (relative maximum in the South) tended to be coincident with the time of deepest MLD, whereas it was 1 month delayed in observations. It is likely that, as discussed for EOF 1, a shallower modeled than observed MLD in March caused an early increase in [Chl] in the North, and an early decrease in the South. After this, a positive peak in the model EOF 3 appeared in spring (April), generally also preceding in 1 month the corresponding peak of the satellite EOF (May). Again an opposite spatial pattern occurred, here corresponding to a [Chl] increase in the northern part of the region, and to a [Chl] decrease south of ∼43° N. The temporal and spatial sequence described suggested that the spring signal captured in EOF 3 corresponded to the second stage of the spring phytoplankton bloom detected in EOF 1. In this stage there was a ‘displacement’ of the bloom from South to North, with [Chl] progressively decreasing south of ∼43° N and progressively increasing to the north of that latitude. This spatio-temporal sequence of the bloom is in agreement with that described by Follows and Dutkiewicz (2001) for the 1998 bloom period over the North Atlantic, and with references therein. It is generally considered a consequence of the ‘critical layer’ mechanism described by Sverdrup (1953) for a light limited water column, i.e., the bloom occurs progresively later in higher latitudes as the insolation increases and the water column stratifies (Follows and Dutkiewicz, 2001). The described differences between the time evolution of [Chl] in the northernmost part of the region and the rest of the region supported the idea that the ocean off West Iberia could be divided in two distinct biogeographic provinces following the classification of Longhurst (1998): most of the region would present characteristics of the Eastern part of North Atlantic Subtropical Gyre (NASTE), whereas the region to the north of ∼43° N would present characteristics of the North Atlantic Drift Province (NADP). Lévy et al. (2005) also described different production regimes in an oceanic region between 16-22° W along West Iberia, characterized by a changing effect of the winter MLD in [Chl] from North to South.

3.3. Cross-correlation analysis

The correlograms of the cross-correlation analyses between the temporal modes of each of the three [Chl] EOFs described and several hydrographic descriptors (model data for both time series) are presented in Figs. 9, 10 and 11. In order to complement the physical descriptors of hydrography, and try to relate them with the nutrients availability, for each of the three EOFs a cross-correlation with the monthly surface NO_3 was also performed.

A strong positive correlation was found between the *spring EOF* and NO_3 at time lag 1 month (Fig. 9). A similar correlation was detected between this EOF and the monthly MLD, indicating that the spring bloom in the model tended to occur one month after the maximum MLD (Fig. 8). However, as previously discussed, in the model the spring bloom occurred 1 month earlier than observed, so we expect the real lag between the maximum MLD and the bloom to be more approximate to 2 months. Note that a positive correlation was also found, at 2 months and 0 time lag, between the *spring EOF* and both the MLD and NO_3. The correlations found suggested a relationship between the winter mixing and the intensity of the subsequent spring bloom, as also proposed by Waniek (2003) from model results. This idea was well exemplified for the years 2005, 2006, and 2009 when maxima in MLD were reached (Fig. 8), coinciding with the years of model [Chl] maxima in the spring bloom (Fig. 4a). However, for 2005 and 2006 the bloom observed from satellite data was not as intense as in the model, in spite of the deeper MLD observed from ARGO floats. We think this is related to the referred anticipation of the March stratification in the model. It is hypothesized that the better model-satellite [Chl] correspondence of 2009 was related to an earlier stratification than usual after the winter mixing (based on ARGO profiles, not shown).

Figure 12 (a) showed the quite homogeneous distribution of this 1 month-lag correlation of the *spring EOF* and the MLD, although with the northern region presenting the highest correlations. The low correlation observed in the shelf region is not significant, because there was a considerable reduction of the data points with MLD values over the shelf. This was a consequence of the imposition of a minimum of 10 m in the calculations of the MLD (see section 2.2), which removed a considerable number of points from the shelf limiting the point to point matches of the spatial comparison. To overcome this, a spatial mean of the monthly MLD was calculated for an area in the shelf (box I; Fig. 1) and a cross-correlation analysis with the *spring EOF* was performed. We obtained a correlation of 0.9 at time lag 1 month, very similar to that obtained for the domain averaged MLD (Fig. 9). This result corroborates that the correlation occurred also for the shelf region.

Figure 10 shows the correlogram between the temporal mode of the *upwelling EOF* of [Chl] and several hydrographic descriptors. A maximum negative correlation (more than -0.6) was found with the SST over the shelf at 0 time lag (after subtracting the seasonal signal of the SST which accounted for more than 90% of the variability; Cordeiro Pires et al. in preparation). This correlation supported the idea that the second source of variability of [Chl] in the Iberian margin was related with the periodic upwelling of cold and nutrient rich ENACW along the Iberian shelf. Note also the positive correlation with NO_3 at 0 lag. The spatial distribution of this correlation (Fig. 12 b) clearly supported the same conclusion. The correlation with the monthly meridional component of the wind (negative sign) over the shelf was similar to that of the SST. This was expected given that the spring-summer upwelling period in western Iberia is known to be driven by prevailing northerly winds (Wooster et al., 1976; Fraga, 1981), increasing [Chl] over the shelf. Still, the correlation coefficient was not as high as it would be expected, attributable to the fact that most of the wind variability is concentrated in periods of < 30 days, with the monthly cycle retaining a low intensity signal (Álvarez-Salgado et al., 2003).

The correlogram between the *winter EOF* and the monthly MLD revealed a negative correlation of -0.6 at time lag 0 (Fig. 11), indicating a co-occurrence of the winter deepening (spring shoaling) of the MLD and a decrease (increase) in [Chl], for the northern part of the domain. The opposite was true for the rest of the region, i.e., a co-occurrence of the winter deepening (spring shoaling) of the MLD and an increase (decrease) in [Chl], since as described in the previous section the EOF 3 captured opposite patterns of [Chl] to the north and south of ∼43° N. A similar negative correlation was found with NO_3 at 0 time lag, indicating the coincidence of the increasing NO_3 concentration and the decreasing [Chl] with the winter MLD deepening (opposite south of 43° N). The 0 time lag correlation between the *winter EOF* and the MLD was higher in some parts of the northern half of the domain (Fig. 12 c). As explained for the *spring EOF* a low correlation was found over the shelf, but it is not representative. Again, a spatial mean of the monthly MLD for the shelf box I (Fig. 1) was calculated and a cross-correlation analysis with the *winter EOF* performed. We found a correlation coefficient of -0.6 at time lag 0, the same correlation found for the domain averaged monthly MLD (Fig. 11).

3.4. [Chl] variability in the water column

The 3D model results allowed to study the biological variability in the water column of the Iberian margin. We focus on the shelf, where short-term highly variable hydrographic conditions (e.g. upwelling, downwelling, continental runoff) overlap the seasonal atmospheric/oceanographic changes, and seem to influence the short-term changes in [Chl] (as seen in Fig. 4 b,d). In particular, a location in the NW Iberian shelf was selected for comparisons with 1-year observations from a sampling station (section 2.2; see position in Fig. 1). This allowed for model evaluation in the water column, and subsequently describe the 10-years interannual [Chl] variability from model results at that location.

3.4.1. Comparison of ROMS outputs with 1-year in situ observations in the NW Iberian shelf

The ability of this ROMS configuration to reproduce the thermohaline properties at this location for the same observational dataset was already discussed, and found satisfactory, in Reboreda et al. (in revision). Therefore, for simplification, we omit here salinity comparisons and refer just to temperature for describing the hydrographic evolution.

Figure 13 presents the observed (a, b, c, d) and modeled (e, f, g, h) water column evolution of temperature, [Chl], NO_3 and NH_4 at a location in the NW Iberian shelf (Fig. 1) between May 2001-April 2002. The seasonal and short-term variability of hydrographic conditions, as represented by the temperature variability, was well captured by the model (Fig. 13 a, e), which showed temperature values very similar to observations.

The model was able to reproduce the recurrent upwelling episodes of the spring-summer period (May-September 2001), breaking the thermal stratification and bringing cold and nitrate rich subsurface ENACW to the surface (Fig. 13 a, e). The higher temporal resolution of the model (daily) allowed a clearer separation of these episodes. The model reproduced the increase in [Chl] immediately after these episodes and the subsequent decrease with the relaxation of the upwelling conditions, even though the [Chl] was higher in model results during most episodes (Fig. 13 b, f). The latter could be, in part, a consequence of the referred higher temporal resolution of model results, given the rapid changes that usually occur in [Chl] in this periods, as shown by the daily surface [Chl] in satellite time series (Fig. 4 b). Still, some higher [Chl] in the model could be attributable to the higher NH_4 simulated by the model (Fig. 13 d, h). It should be noted that the model lacked a dissolved organic nitrogen (DON) compartment, so the modeled NH_4 distribution was probably representing in part the DON distribution. On the other hand, the high NO_3 observed in the subsurface cold ENACW was well reproduced by the model (Fig. 13 c, g). At the end of September a strong downwelling event occurred, that was also appropriately reproduced by the model, as a consequence of the seasonal shift in the wind direction to southwesterlies, which brought warm (>17°C) and nitrate poor (<1 mmol N m^{-3}) surface offshore water into the shelf (Fig. 13 a, c, e, g). It was associated to a pronounced decrease in [Chl] as shown by observations and model results, which presented similar concentration values (Fig. 13 b, f) and an increase in NH_4 in the water column (Fig. 13 d, h), presumably due to downward advection of organic matter and its subsequent mineralization. The out-of-season strong upwelling event of November 2001, which introduced cold and highly nitrate rich subsurface ENACW into the sea surface, causing an unusual strong phytoplankton bloom for this time of the year, was also reproduced by the model. However, the [Chl] maxima was delayed relative to observations (Fig. 13 a, b, c, e, f, g). After this event, the wind regime returned to the typical southwesterlies of this time of the year, coinciding with a warming of the water column due to the onset of the IPC over the Iberian slope, conveying warm and saline ENACW of subtropical origin (ENACWt). The dominant downwelling/IPC situation prevailed until February, characterized by low [Chl] (∼0.5 mg m^{-3}) in both observations and model results (Fig. 13 b, f). During late February-March 2002 the model reproduced the winter mixing of the water column. Then, a first phytoplankton bloom occurred in the still homogeneous water column, before the spring thermal stratification, also reproduced by the model, although with lower [Chl] and a delayed maximum. It has been argued that these kind of spring blooms in the absence of stratification are a consequence of deep penetration of light in relatively clear late-winter waters (Townsend et al., 1992). In late March, the model reproduced the haline stratification caused by a river plume (not shown), which seemed to coincide with a surface intensification of the bloom (Fig. 13 b, f). Finally, the thermal spring stratification developed in April, under upwelling favorable conditions, giving rise to a new phytoplankton bloom which seemed to be somehow weaker in the model.

3.4.2. Interannual variability : ROMS simulation of 10-years biogeochemical evolution in the NW Iberian shelf

ROMS outputs were used to reconstruct the water column [Chl] variability, together with other biogeochemical variables and thermohaline properties, at the shelf location just described (Fig. 1) for the 10 years period (2001-2010) (Fig. 14). Note that the detail of the variability is coarser here than for the description of 2001-2002, as a 30-day running mean was applied in order to smooth the small scale variability for a much longer period and to make it easier to interpret. As expected, the spring-summer [Chl] (phytoplankton) blooms, driven by the upwelling pulses of cold and nitrate rich ENACW, were the main source of [Chl] variability throughout the years. Interannual differences in the upwelling intensity and persistence could be inferred from the temperature and [Chl] distribution, showing years of clearly separated upwelling pulses, as 2005, and years of more persistent stratification, as 2003, when surface [Chl] was lower than usual (Fig. 14 a, b). Modeled [Chl] was also lower than usual in 2009 and 2010, but this has already been interpreted as a possible adjustment to the shift in the surface model forcing (section 3.1). Out-of-season strong upwelling events, such as that of November 2001, that can be captured with a 30-day running mean, did not seem to be frequent. The autumn shift to prevailing downwelling conditions was clearly detectable every year from the surface warming and the decrease in [Chl] (Fig. 14 a, b). This shift could be more abrupt, as in 2002 and 2006, or it could be more gradual, as in 2005. From that time to the beginning of the next year (autumn-winter) the presence of the IPC over the slope was also reflected in the thermohaline properties of the shelf waters (more saline and warm; Fig. 14 b, c). This period was also characterized by a gradual increase in [Chl] until a phytoplankton bloom occurred, either coinciding with the maximum of vertical homogenization of the winter mixing (sharp temperature decrease), as in 2001 and 2003, or with the spring stratification, as in 2005 and 2006.

Trends in [Chl] and temperature, for the upper 10 m of the water column and the 10 m above the bottom, were studied at this shelf location for the period 2001-2010. Linear trends were calculated considering the annual anomalies and also the anomalies of the summer upwelling period (April-September) and the winter downwelling period (October-March) separately. The slope of these regression analyses are presented in Table 4. There was a significant positive trend in temperature, considering the annual anomalies, both in the upper water column and in the bottom, however the trend was not significant when considering the upwelling/downwelling periods separately, except the bottom temperature for the upwelling period. A slightly negative trend was found in the upper water column [Chl], but it was not significant. Note that the significant trends found for temperature should be taken with caution, because of the short period tested (10 years) and the change in the surface forcing used for model simulations of the last two years, with the implications already discussed.

4. Summary and conclusions

The capability of the ROMS configuration, coupled to a N_2PZD_2-type biogeochemical model, to reproduce the [Chl] variability in the study region has been satisfactorily tested. The model was able to reproduce the observed (satellite derived) seasonal variability on [Chl] at the sea surface in the Iberian margin for the decade 2001-2010. It was also able to reproduce the observed vertical short-term variability of [Chl], NO_3 and thermohaline properties on the shelf along 1-year cycle. It thus provides a useful tool, presenting potentialities for further research and as an operational product for the marine community. The model presented however some limitations that should be taken into account for future applications. Namely, the anticipation of the spring phytoplankton bloom in about 1 month, higher [Chl] than observed during the bloom, and slightly lower concentrations than observed along the rest of the year. However, the statistical analysis of these differences showed that they were quite variable from year to year over the study period. This highlighted the influence of the surface (atmospheric) forcing on the results of the biogeochemical model. On the other hand, the use of climatological [Chl] at the lateral boundaries, with only seasonal variability (4 values/year), is certainly a limitation of the model when running an interannual simulation. More efforts to satisfactorily implement a biogeochemical model in the outer domain (FD) are needed, so that it could give higher resolution information for the biogeochemical variables to the SD. The use of constant nitrate concentration values for the rivers does not properly represent the nutrient input to the shelf from continental runoff. Model results would benefit from the availability of more realistic continental nitrate inputs.

Three main modes of sea surface [Chl] variability were found for the western Iberia oceanic and shelf regions, both from EOF analysis of model results and satellite observations, which represented the seasonal variability in the region (monthly time scale). The first one, which we named the *spring EOF* because of the evident spring (March-April) signal in the temporal mode, explained 69.25% of [Chl] variability in the model and 46.32% of variability in the remotely sensed [Chl]. The second source of variability (EOF 2) explained 14.45% of modeled vs. 26.54% of observed [Chl] variability, and was found to be related to the spring-summer increase in [Chl] over the shelf during the upwelling season (*upwelling EOF*). The EOF 3 explained 9.67% of modeled [Chl] variability and 13.42% of the observed variability, and we named it the *winter EOF* because the strongest signal in the temporal mode was a minimum in winter (February), although it also presented a positive signal in spring (March-April). The cross-correlation analyses showed that the MLD had a strong positive correlation with the *spring EOF* at time lag 1 month, and a negative correlation with the *winter EOF* at 0 time lag. This revealed a possible double (and opposite) effect of the MLD on the seasonal evolution of [Chl] in the western Iberia. On one hand the deepening of the MLD during the winter mixing seemed to be related with the intensity of [Chl] increase (spring bloom) in the subsequent months, particularly in the northern part of the region, where the winter MLD gets deeper (up to 300 m). On the other hand, there seemed to be a synchronization of the winter MLD deepening (spring shoaling) and [Chl] decrease (increase) north of $\sim$43° N. South of that latitude the deepening of winter MLD coincided with a [Chl] increase, reaching a maximum in late winter/early spring (February-March), after which the [Chl] decreased as the MLD started shoaling (March-April) and the surface nutrients were used. At the same time, the bloom in the North was progressively intensified as the deep winter MLD disappeared by the spring stratification, giving the impression of a South-to-North displacement of the bloom. Thus, the proposed opposite influence of the MLD on

[Chl] would present both a time and a spatial dependence, supporting the existence of two production regimes off western Iberia, to the north and south of ∼43° N, with differing time evolution of [Chl]. This would help to explain some apparently contradictory observations of the literature Peliz and Fiuza (1999), giving a more complete picture of the seasonal evolution of [Chl] over the region. The commonly accepted idea that offshore [Chl] throughout winter decreases, just increasing in spring, should be reconsidered.

The summer upwelling production regime characterized the Iberian shelf, which for the 10 years time-span analyzed was the second source of [Chl] variability (when considering the entire domain, i.e., the shelf and offshore region). The *upwelling EOF* of [Chl] was negatively correlated with the meridional wind and SST (and positively correlated with NO_3) over the shelf. This result is in agreement with the analysis of Álvarez-Salgado et al. (2002) for the period 1982-1999, showing that 83% of the variability of new production in the northwestern Iberian shelf was explained by the offshore Ekman transport (i.e., it was related to the upwelling).

In accordance with the results for the surface, the water column [Chl] variability over the shelf for the study period was mainly influenced by the interannual intensity and persistence of the upwelling. The autumn shift to prevailing downwelling conditions tended to decrease [Chl] over the shelf. The timing for this transition was quite variable from year to year. The spring phytoplankton blooms reproduced by the model occurred both in conditions of vertical homogeneity (2001, 2003) or coinciding with the spring stratification (2005, 2006). Thus, as expected, the short-term variability in the shelf seemed to play a more relevant role, which needs to be further explored in future studies, taking advantage of the modeling possibilities demonstrated here.

5. Acknowledgements

This research has been supported by the Portuguese *Fundação para a Ciencia e a Tecnologia* (FCT) through a PhD grant to R.R. (SFRH /BD /33388 /2008). The work has been developed within the frame of the RAIA project (Observatorio oceánico del margen Ibérico, POCTEP-FEDER, 0520_RAIA_CO_1_E), which financed a research fellowship to N.G.F.C. The results of this work contributed partially to the objectives of the project HAB-SPOT (Harmful Algal Bloom dynamics - Shelf Processes of Transport and retention Offshore Aveiro, PTDC/MAR/100348/2008). X.A.A.S. was funded by the project CAIBEX (Shelf-ocean exchanges in the Canaries-Iberian Large Marine Ecosystem, grant No CTM2007-66408-C02-01/MAR). We are thankful to the Spanish *Consejo Superior de Investigaciones Científicas* (CSIC) for providing the data of the station sampled within the frame of the DYBAGA project (grant No MAR99-1039-C02-01). Thank you to the IFREMER/CERSAT for the free availability of the satellite chlorophyll products used in this study. We also thank the Portuguese *Instituto Nacional da Água* (INAG) for free access to the available data on river discharges.

References

Albert, A., Echevin, V., Levy, M., Aumont, O., 2010. Impact of nearshore wind stress curl on coastal circulation and primary productivity in the Peru upwelling system. Journal of Geophysical Research-Oceans 115, C12033, doi:10.1029/2010jc006569.

Allen, J. I., Holt, J. T., Blackford, J., Proctor, R., 2007. Error quantification of a high-resolution coupled hydrodynamic-ecosystem coastal-ocean model: Part 2. Chlorophyll-a, nutrients and SPM. Journal of Marine Systems 68, 381–404.

Álvarez-Salgado, X. A., Beloso, S., Joint, I., Nogueira, E., Chou, L., Perez, F. F., Groom, S., Cabanas, J. M., Rees, A. P., Elskens, M., 2002. New production of the NW Iberian shelf during the upwelling season over the period 1982-1999. Deep-Sea Research Part I-Oceanographic Research Papers 49 (10), 1725–1739.

Álvarez-Salgado, X. A., Figueiras, F. G., Perez, F. F., Groom, S., Nogueira, E., Borges, A., Chou, L., Castro, C. G., Moncoiffe, G., Rios, A. F., Miller, A. E. J., Frankignoulle, M., Savidge, G., Wollast, R., 2003. The Portugal coastal counter current off NW Spain: new insights on its biogeochemical variability. Progress in Oceanography 56 (2), 281–321.

Álvarez-Salgado, X. A., Nieto-Cid, M., Gago, J., Brea, S., Castro, C. G., Doval, M. D., Perez, F. F., 2006. Stoichiometry of the degradation of dissolved and particulate biogenic organic matter in the NW Iberian upwelling. Journal of Geophysical Research-Oceans 111, C07017, doi:10.1029/2004jc002473.

Arhan, M., de Verdière, A. C., Memery, L., 1994. The eastern boundary of the subtropical North-Atlantic. Journal of Physical Oceanography 24 (6), 1295–1316.

Bode, A., Anadon, R., Moran, X. A. G., Nogueira, E., Teira, E., Varela, M., 2011. Decadal variability in chlorophyll and primary production off NW Spain. Climate Research 48, 293–305.

Bode, A., Casas, B., Fernandez, E., Maranon, E., Serret, P., Varela, M., 1996. Phytoplankton biomass and production in shelf waters off NW Spain: Spatial and seasonal variability in relation to upwelling. Hydrobiologia 341 (3), 225–234.

Castro, C. G., Alvarez-Salgado, X. A., Figueiras, F. G., Perez, F. F., Fraga, F., 1997. Transient hydrographic and chemical conditions affecting microplankton populations in the coastal transition zone of the Iberian upwelling system (NW Spain) in September 1986. Journal of Marine Research 55 (2), 321–352.

Chen, C. A., Liu, K. K., Macdonald, R., 2003. Continental Margin Exchanges. In: Fasham, M. J. R. (Ed.), Ocean Biogeochemistry. Springer-Verlag, pp. 53–95.

de Boyer Montégut, C., Madec, G., Fischer, A. S., Lazar, A., Iudicone, D., 2004. Mixed layer depth over the global ocean: An examination of profile data and a profile-based climatology. Journal of Geophysical Research 109, C12003, doi:10.1029/2004JC002378.

Echevin, V., Aumont, O., Ledesma, J., Flores, G., 2008. The seasonal cycle of surface chlorophyll in the peruvian upwelling system: A modelling study. Progress in Oceanography 79 (2-4), 167–176.

Espinoza-González, O., Figueiras, F. G., Crespo, B. G., Teixeira, I. G., Castro, C. G., 2012. Autotrophic and heterotrophic microbial plankton biomass in the NW Iberian upwelling: seasonal assessment of metabolic balance. Aquatic Microbial Ecology 67, 77–89.

Figueiras, F. G., Labarta, U., Reiriz, M. J. F., 2002. Coastal upwelling, primary production and mussel growth in the Rias Baixas of Galicia. Hydrobiologia 484 (1-3), 121–131.

Follows, M., Dutkiewicz, S., 2001. Meteorological modulation of the North Atlantic spring bloom. Deep Sea Research Part II: Topical Studies in Oceanography 49, 321 – 344.

Fraga, F., 1981. Upwelling off the Galician coast, Northwest Spain. In: Richards, S. A. (Ed.), Coastal upwelling series. Vol. 1. AGU, Washington DC, pp. 176–182.

Garcia, H. E., Locarnini, R. A., Boyer, T., Antonov, J., Zweng, M., Baranova, O., Johnson, D., 2010. World Ocean Atlas 2009, volume 4: Nutrients (phosphate, nitrate, silicate).

Geider, R. J., MacIntyre, H. L., Kana, T. M., 1997. Dynamic model of phytoplankton growth and acclimatation: responses of the balanced growth rate and the chlorophyll a:carbon ratio to light, nutrient-limitation and temperature. Marine Ecology Progress Series 148, 187–200.

Glover, D. M., Jenkins, W. J., Doney, S., 2011. Modeling Methods for Marine Science. Cambridge University Press, Cambridge, UK.

Gregg, W. W., Casey, N. W., 2007. Sampling biases in MODIS and SeaWIFS ocean chlorophyll data. Remote Sensing of the Environment 111, 25–35.

Gruber, N., Frenzel, H., Doney, S. C., Marchesiello, P., McWilliams, J. C., Moisan, J. R., Oram, J. J., Plattner, G. K., Stolzenbach, K. D., 2006. Eddy-resolving simulation of plankton ecosystem dynamics in the California Current System. Deep-Sea Research Part I-Oceanographic Research Papers 53 (9), 1483–1516.

Haidvogel, D. B., Arango, H., Budgell, W. P., Cornuelle, B. D., Curchitser, E., Di Lorenzo, E., Fennel, K., Geyer, W. R., Hermann, A. J., Lanerolle, L., Levin, J., McWilliams, J. C., Miller, A. J., Moore, A. M., Powell, T. M., Shchepetkin, A. F., Sherwood, C. R., Signell, R. P., Warner, J. C., Wilkin, J., 2008. Ocean forecasting in terrain-following coordinates: Formulation and skill assessment of the regional ocean modeling system. Journal of Computational Physics 227 (7), 3595–3624.

Haynes, R., Barton, E. D., 1990. A poleward flow along the Atlantic coast of the Iberian Peninsula. Journal of Geophysical Research-Oceans 95 (C7), 11425–11441.

Herrera, J. L., Rosón, G., Varela, R. A., Piedracoba, S., 2008. Variability of the western Galician upwelling system (NW Spain) during an intensively sampled annual cycle. An EOF analysis approach. Journal of Marine Systems 72 (14), 200–217.

Holte, J., Gilson, J., Talley, L., Roemmich, D., 2010. Argo Mixed Layers. Scripps Institution of Oceanography/UCSD. http://mixedlayer.ucsd.edu.

Holte, J., Talley, L., 2009. A new algorithm for finding mixed layer depths with applications to Argo data and Subantarctic Mode Water formation. Journal of Atmospheric and Oceanic Technology 26, 1920–1939.

Joint, I., Groom, S. B., Wollast, R., Chou, L., Tilstone, G. H., Figueiras, F. G., Loijens, M., Smyth, T. J., 2002. The response of phytoplankton production to periodic upwelling and relaxation events at the Iberian shelf break: estimates by the c-14 method and by satellite remote sensing. Journal of Marine Systems 32 (1-3), 219–238.

Koné, V., Machu, E., Penven, P., Andersen, V., Garcon, V., Fréon, P., Demarcq, H., 2005. Modeling the primary and secondary productions of the southern Benguela upwelling system: A comparative study through two biogeochemical models. Global Biogeochemical Cycles 19 (4), GB4021, doi:10.1029/2004GB002427.

Le Fouest, V., Zakardjian, B., Saucier, F., Cizmeli, S. C., 2006. Application of seawifs- and avhrr-derived data for mesoscale and regional validation of a 3-d high-resolution physical-biological model of the gulf of st. lawrence (canada). Journal of Marine Systems 60, 30 – 50.

Lévy, M., Lehahn, Y., André, J. M., Mémery, L., Loisel, H., Heifetz, E., 2005. Production regimes in the northeast Atlantic: A study based on Sea-viewing Wide Field-of-view Sensor (SeaWiFS) chlorophyll and ocean general ciruculation model mixed layer depth. Journal of Geophysical Research 110, C07S10, doi:10.1029/2004jc002771.

Longhurst, A. R., 1998. Ecological Geography of the Sea. Academic Press.

Machu, E., Biastoch, A., Oschlies, A., Kawamiya, M., Lutjeharms, J. R. E., Garcon, V., 2005. Phytoplankton distribution in the agulhas system from a coupled physical-biological model. Deep-Sea Research Part I-Oceanographic Research Papers 52 (7), 1300–1318.

Marta-Almeida, M., Reboreda, R., Rocha, C., Dubert, J., Nolasco, R., Cordeiro, N., Luna, T., Rocha, A., Lencart e Silva, J. D., Queiroga, H., Peliz, A., Ruiz-Villarreal, M., 2012. Towards operational modeling and forecasting of the iberian shelves ecosystem. PLoS ONE 7 (5), e37343.

Miles, T. N., He, R., 2010. Temporal and spatial variability of Chl-a and SST on the South Atlantic Bight: Revisiting with cloud-free reconstructions of MODIS satellite imagery. Continental Shelf Research 30 (18), 1951 – 1962.

Morel, A., Berthon, J. F., 1989. Surface pigments, algal biomass profiles, and potential production of the euphotic layer: Relationships reinvestigated in view of remote-sensing application. Limnology and Oceanography 34, 1545–1562.

Nieto-Cid, M., Alvarez-Salgado, X. A., Brea, S., Perez, F. F., 2004. Cycling of dissolved and particulate carbohydrates in a coastal upwelling system (NW Iberian Peninsula). Marine Ecology-Progress Series 283, 39–54.

Nolasco, R., Pires, A., Cordeiro, N., Cann, B., Dubert, J., 2013. A high-resolution modeling study of the western iberian margin mean and seasonal upper ocean circulation. Ocean Dynamics 63 (9-10), 1041–1062.

Oliveira, P., Moita, T., Catarino, R., da Silva, A. J., 2007. Wintertime SST and Chla off NW Iberian shelf from satellite and insitu data. In: Joint 2007 EUMETSAT Meteorological Satellite Conference and the 15th Satellite Meteorology & Oceanography Conference of the American Meteorological Society. Amsterdam, The Netherlands.

Oliveira, P. B., Nolasco, R., Dubert, J., Moita, T., Peliz, A., 2009. Surface temperature, chlorophyll and advection patterns during a summer upwelling event off central Portugal. Continental Shelf Research 29 (5-6), 759–774.

Otero, P., Ruiz-Villarreal, M., Garcia-Garcia, L., Marta-Almeida, M., Cobas, M., Gonzalez-Nuevo, G., Cabanas, J. M., June 2011. Walking on the sea side: Modeling and observational efforts of the iberian margin ocean observatory (raia). In: OCEANS, 2011 IEEE - Spain. pp. 1–6.

Peliz, A., Dubert, J., Marchesiello, P., Teles-Machado, A., 2007. Surface circulation in the Gulf of Cadiz: Model and mean flow structure. Journal of Geophysical Research-Oceans 112, C11015, doi:10.1029/2007jc004159.

Peliz, A., Dubert, J., Santos, A. M. P., Oliveira, P. B., Le Cann, B., 2005. Winter upper ocean circulation in the Western Iberian Basin - fronts, eddies and poleward flows: an overview. Deep-Sea Research Part I-Oceanographic Research Papers 52 (4), 621–646.

Peliz, A., Marchesiello, P., Santos, A. M. P., Dubert, J., Teles-Machado, A., Marta-Almeida, M., Le Cann, B., 2009. Surface circulation in the Gulf of Cadiz: 2. Inflow-outflow coupling and the Gulf of Cadiz slope current. Journal of Geophysical Research-Oceans 114 (C3), doi:10.1029/2008JC004771.

Peliz, A., Rosa, T. L., Santos, A. M. P., Pissarra, J. L., 2002. Fronts, jets, and counter-flows in the Western Iberian upwelling system. Journal of Marine Systems 35 (1-2), 61–77.

Peliz, A. J., Fiuza, A. F. G., 1999. Temporal and spatial variability of CZCS-derived phytoplankton pigment concentrations off the western Iberian Peninsula. International Journal of Remote Sensing 20 (7), 1363–1403.

Penven, P., Debreu, L., Marchesiello, P., McWilliams, J. C., 2006. Evaluation and application of the ROMS 1-way embedding procedure to the central California upwelling system. Ocean Modelling 12 (1-2), 157–187.

Perez, F. F., Castro, C. N. G., Rios, A. F., Fraga, F., 2005. Chemical properties of the deep winter mixed layer in the Northeast Atlantic (40-47 degrees N). Journal of Marine Systems 54 (1-4), 115–125.

Preisendorfer, R. W., 1988. Principal Component Analyses in Meteorology and Oceanography. Elsevier.

Reboreda, R., Castro, C. G., Álvarez-Salgado, X. A., Nolasco, R., Cordeiro, N. G. F., Queiroga, H., Dubert, J., in revision. Oxygen in the iberian margin: a modelling study. Progress in Oceanography.

Relvas, P., Barton, E. D., Dubert, J., Oliveira, P. B., Peliz, A., da Silva, J. C. B., Santos, A. M. P., 2007. Physical oceanography of the western Iberia ecosystem: Latest views and challenges. Progress in Oceanography 74 (2-3), 149–173.

Ribeiro, A. C., Peliz, A., Santos, A. M. P., 2005. A study of the response of chlorophyll-a biomass to a winter upwelling event off western Iberia using SeaWiFS and in situ data. Journal of Marine Systems 53 (1-4), 87–107.

Río-Barja, F., Rodríguez-Lestegás, F., 1992. Os ríos galegos. Morfoloxía e réxime. Consello da Cultura Galega, Santiago de Compostela.

Sánchez, R. F., Relvas, P., Delgado, M., 2007. Coupled ocean wind and sea surface temperature patterns off the western Iberian Peninsula. Journal of Marine Systems 68, 103 – 127.

Santos, A. M. P., Kazmin, A. S., Peliz, A., 2005. Decadal changes in the Canary Upwelling System as revealed by satellite observations: Their impact on productivity. Journal of Marine Research 63 (2), 359–379.

Saulquin, B., Gohin, F., Garrello, R., 2011. Regional objective analysis of merging high-resolution MERIS, MODIS/Aqua, and SeaWIFS chlorophyll-a data from 1998 to 2008 on the European Atlantic Shelf. IEEE Transactions on Geoscience and Remote Sensing 49 (1), 143–154.

Serra, N., Ambar, I., Boutov, D., 2010. Surface expression of Mediterranean Water dipoles and their contribution to the shelf/slope-open ocean exchange. Ocean Science 6(1), 191–209.

Shchepetkin, A. F., McWilliams, J. C., 2005. The regional oceanic modeling system (ROMS): a split-explicit, free-surface, topography-following-coordinate oceanic model. Ocean Modelling 9 (4), 347–404.

Shutler, J. D., Smyth, T. J., Saux-Picart, S., Wakelin, S. L., Hyder, P., Orekhov, P., Grant, M. G., Tilstone, G. H., Allen, J. I., 2011. Evaluating the ability of a hydrodynamic ecosystem model to capture inter- and intra-annual spatial characteristics of chlorophyll-a in the north east Atlantic. Journal of Marine Systems 88, 169–182.

Silva, A., Palma, S., Oliveira, P. B., Moita, M. T., 2009. Calcidiscus quadriperforatus and calcidiscus leptoporus as oceanographic tracers in lisbon bay (portugal). Estuarine, Coastal and Shelf Science 81 (3), 333–344.

Stow, C. A., Jolliff, J., McGillicuddy, D. J., Doney, S. C., Allen, J. I., Friedrichs, M. A. M., Rose, K. A., Wallheadg, P., 2009. Skill assessment for coupled biological/physical models of marine systems. Journal of Marine Systems 76 (1-2), 4–15.

Sverdrup, H. U., 1953. On conditions for the vernal blooming of phytoplankton. Journal du Conseil International pour l'Exploration de la Mer 18 (3), 287–295.

Tenore, K. R., Alonso-Noval, M., Alvarez-Ossorio, M., Atkinson, L. P., Cabanas, J. M., Cal, R. M., Campos, H. J., e. a., 1995. Fisheries and oceanographiy off Galicia, NW Spain (FOG): mesoscale spatial and temporal changes in physical processes and resultant patterns of biological productivity. Journal of Geophysical Research 100, 10943–10966.

Townsend, D. W., Keller, M. D., Sieracki, M. E.and Ackleson, S. G., 1992. Spring phytoplankton blooms in the absence of vertical water column stratification. Letters to Nature 360, 59.

Waniek, J. J., 2003. The role of physical forcing in initiation of spring blooms in the northeast Atlantic. Journal of Marine Systems 39, 57 – 82.

Warner, J. C., Geyer, W. R., Lerczak, J. A., 2005. Numerical model of an estuary: A comprehensive skill assessment. Journal of Geophysical Research-Oceans 110, C05001, doi:10.1029/2004jc002691.

Williams, R. G., Follows, M., 2003. Physical transport of nutrients and maintenance of biological production. In: Fasham, M. J. R. (Ed.), Ocean Biogeochemistry. Springer-Verlag, pp. 19–49.

Wooster, W. S., Bakun, A., Mclain, D. R., 1976. Seasonal upwelling cycle along Eastern boundary of North-Atlantic. Journal of Marine Research 34 (2), 131–141.

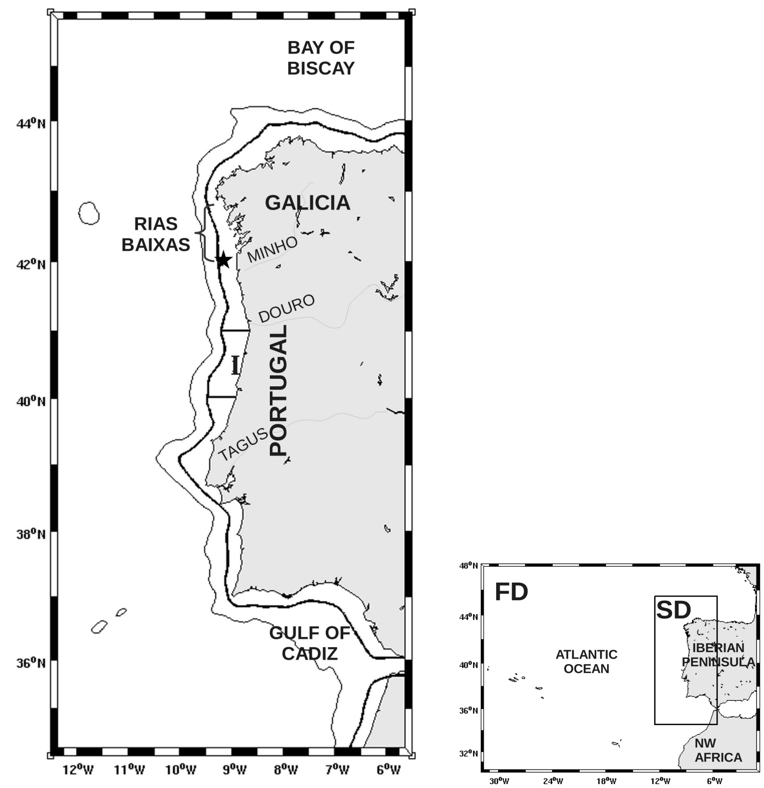

Figure 1: Region of study and nested model domains. Target domain (left), with indication of the parent domain used to provide lateral boundaries (right). FD stands for First Domain and SD stands for Second Domain. Model isobaths of 200 m (black line) and 1000 m (gray line) are depicted (real depth smoothed). Box I indicates the shelf region used for time series comparisons in section 3.1. The star shows the location of the shelf station used to compare water column observations with model outputs.

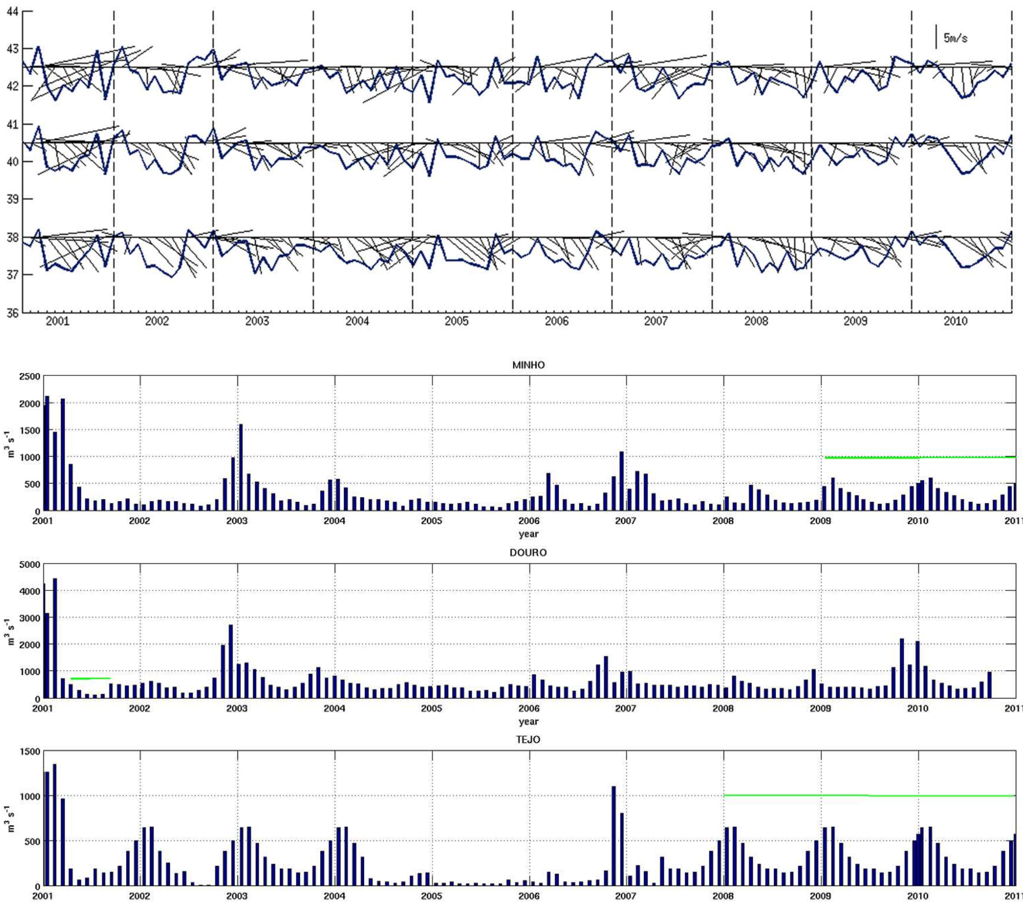

Figure 2: Local forcings in the Iberian shelf (2001-2010). Upper panel: Monthly time series of QuikSCAT (2001-2008) and ASCAT (2009-2010) wind velocity and direction (black sticks) and meridional component (solid line) at three locations along the Iberian shelf (9.5° W): 38° N, 40.5° N and 42.5° N; Lower panel: Monthly continental runoff from the main rivers: Douro, Minho, and Tagus (m^3 s^{-1}; note different scales). Green lines over the bars indicate climatological values, otherwise values are averaged from real daily discharges.

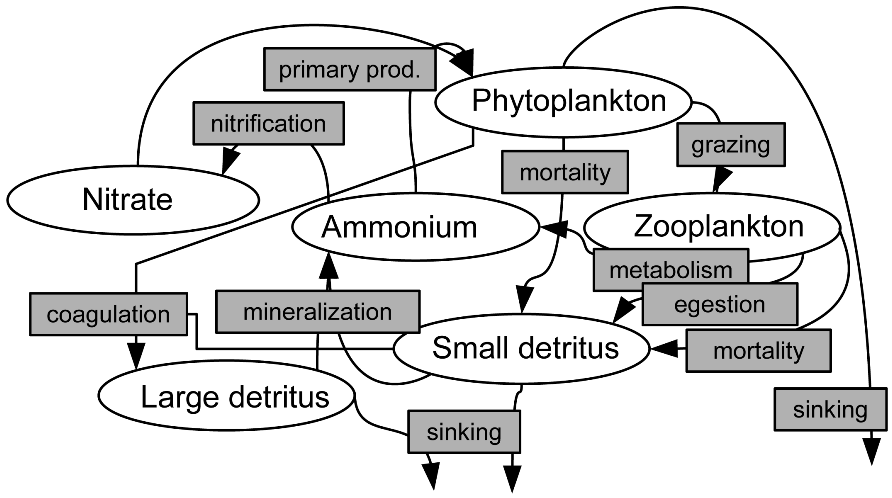

Figure 3: Diagram of the N_2PZD_2 model. Model state variables (NO_3, NH_4, $Phyt$, Zoo, $SDet$ and $LDet$) are represented in terms of nitrogen concentration.

	Description	Reference
T	Temperature	
PAR	Photosynthetically Available Radiation	Koné et al. (2005)
$\mu(PAR, T)$	light dependent, temperature limeted growth rate	Gruber et al. (2006)
$\mu(NO_3, NH_4)$	nutrient limitation factor	Gruber et al. (2006)
$t_{NH4_{nitr}}\ NH_4$	ammonification	Gruber et al. (2006)
$t_{Z_{metab}}\ Zoo$	zooplankton excretion of ammonium	Gruber et al. (2006)
$t_{SD_{remin}}\ SDet$	mineralization of slow sinking detritus	Gruber et al. (2006)
$t_{LD_{remin}}\ LDet$	mineralization of fast sinking detritus	Gruber et al. (2006)
$m_{PD}\ Phyt$	phytoplankton mortality	Gruber et al. (2006)
$g_{max}\ Zoo\ \frac{Phyt}{K_P+Phyt}$	zooplankton grazing on phytoplankton	Gruber et al. (2006)
$m_{ZD}\ Zoo$	zooplankton mortality	Koné et al. (2005)
$(1-\beta)\ g_{max}\ Zoo\ \frac{Phyt}{K_P+Phyt}$	egestion of fecal pellets	Koné et al. (2005)
$Sagg \cdot (Phyt + SDet)^2$	particle coagulation	Gruber et al. (2006)

Table 1: Description and references for the terms of the biogeochemical SMS equations listed in section 2.1.2

.

Parameter		Value	Unit
K_w	Light attenuation in seawater	0.04	m^{-1}
K_{chla}	Light attenuation by chlorophyll	0.024	$(m^2 \text{ mg Chla})^{-1}$
α	Initial slope of the P-I curve	1	mg C (mg ChlaW m^{-2} d)$^{-1}$
θ_{max}	Maximum cellular chlorophyll:C ratio	0.03	mg Chla(mg C)$^{-1}$
K_{NO3}	Half-saturation for phytoplankton NO_3 uptake	0.9	mmol N m^{-3}
K_{NH4}	Half-saturation for phyoplankton NH_4 uptake	0.5	mmol N m^{-3}
K_P	Zooplankton half-saturation constant for ingestion	1	mmol N m^{-3}
g_{max}	Maximum zooplankton growth rate	0.6	d^{-1}
β	Zooplankton assimilation coefficient	0.75	n.d.
m_{PD}	Phytoplankton mortality rate to small detritus	0.072	d^{-1}
m_{ZD}	Zooplankton mortality rate to small detritus	0.025	d^{-1}
t_{Zmetab}	Zooplankton specific excretion rate	0.1	d^{-1}
$t_{SDremin}$	Small detritus mineralization to NH_4 rate	0.03	d^{-1}
$t_{LDremin}$	Large detritus mineralization to NH_4 rate	0.01	d^{-1}
$t_{NH4nitr}$	NH_4 nitrification rate	0.05	d^{-1}
S_{agg}	Specific aggregation rate (Phyt + SDet)	0.005	(mmol N d)$^{-1}$
w_P	Sinking velocity for phytoplankton	0.5	m d^{-1}
w_{LD}	Sinking velocity for large detritus	10	m d^{-1}
w_{SD}	Sinking velocity for small detritus	1	m d^{-1}

Table 2: Parameter values of the $N_2ChlPZD_2$ model.

	bias	rms	skew	skill
2001	-0.277	0.183	-0.046	0.716
2002	-0.08	0.207	0.031	0.64
2003	-0.191	0.15	-0.013	0.786
2004	0.003	0.164	0.039	0.805
2005	0.057	0.35	0.101	0.617
2006	-0.026	0.283	0.085	0.532
2007	-0.226	0.182	-0.035	0.574
2008	-0.143	0.203	-0.037	0.639
2009	-0.335	0.239	-0.061	0.853
2010	-0.365	0.231	-0.055	0.637

Table 3: Error statistics of model-satellite comparisons for domain averaged daily [Chl] time series.

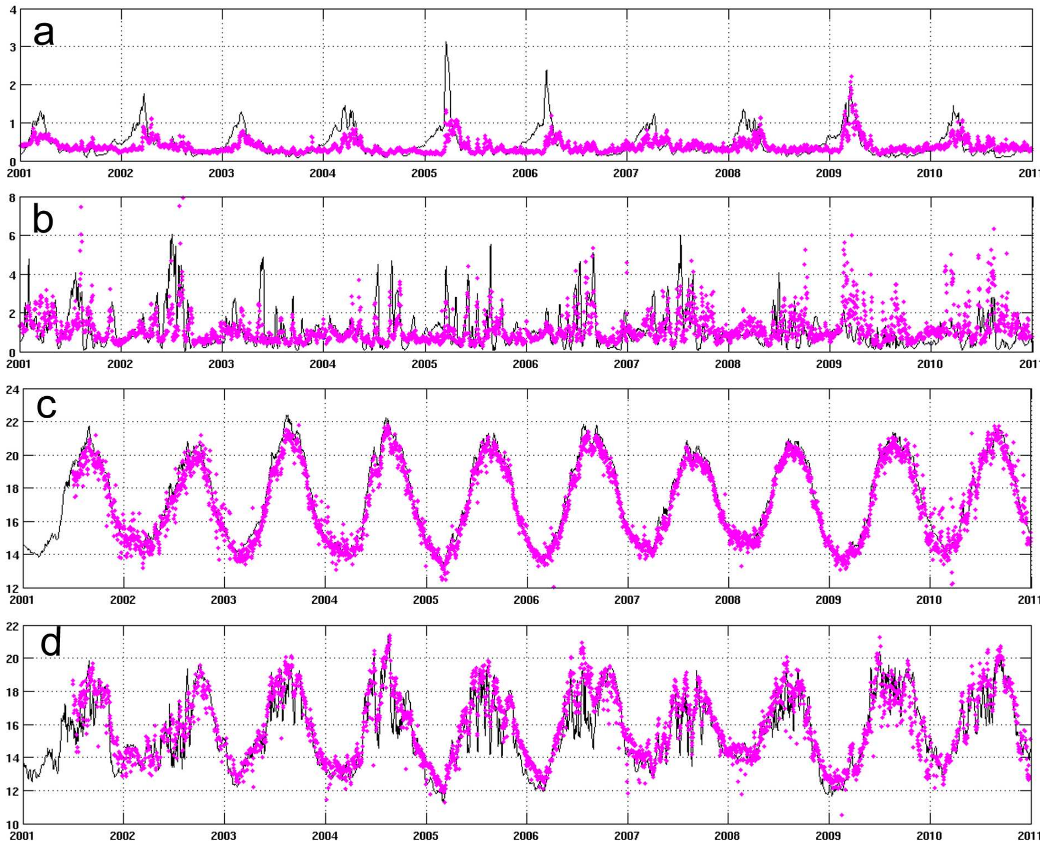

Figure 4: Time series of daily surface [Chl] (mg m^{-3}) and SST from model outputs (solid line) and satellite observations (dots): a) domain averaged [Chl]; b) central shelf (box I Fig.1) averaged [Chl]; c) domain averaged SST; d) central shelf (box I Fig.1) averaged SST.

	[Chl] (mg m^{-3} year^{-1})		**Temperature (ºC year^{-1})**	
	Upper 10 m	Bottom 10 m	Upper 10 m	Bottom 10 m
Upwelling season	-0.07	0.001	0.14	0.1*
Winter season	-0.02	0.0002	0.1	0.04
Annual	-0.04	0.001	0.09*	0.08*

Table 4: Trends in [Chl] and temperature for the upper 10 m of the water column and the 10 m above the bottom at the shelf station in Fig 1. Analysis based on annual, upwelling season (April-September), and downwelling season (October-March) anomalies fitting to a straight line. $^*p < 0.05$

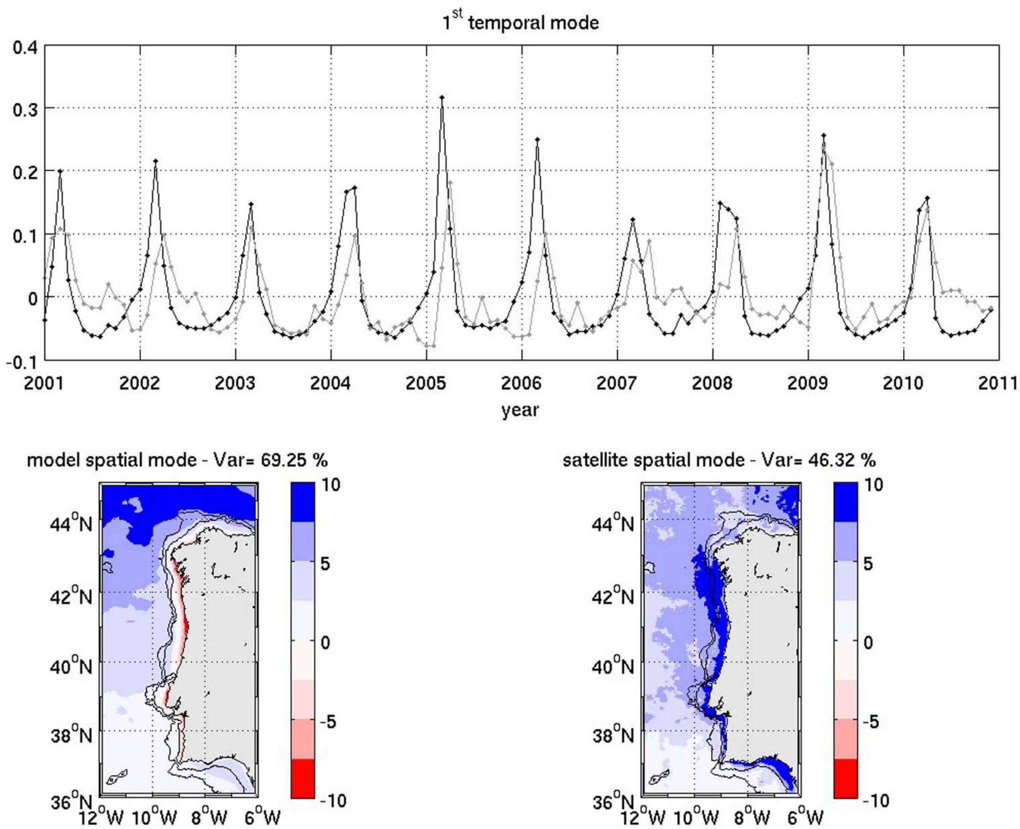

Figure 5: First mode of temporal (upper panel) and spatial (lower panel) variability from the EOF analysis of domain averaged surface [Chl] (monthly means): comparison between model outputs (black line in temporal mode, left panel in spatial field) and satellite observations (gray line in temporal mode, right panel in spatial field). Points in the time series represent months from January to December. Same temporal and spatial sign (+/−) means increase in [Chl] (decrease when sign is opposite).

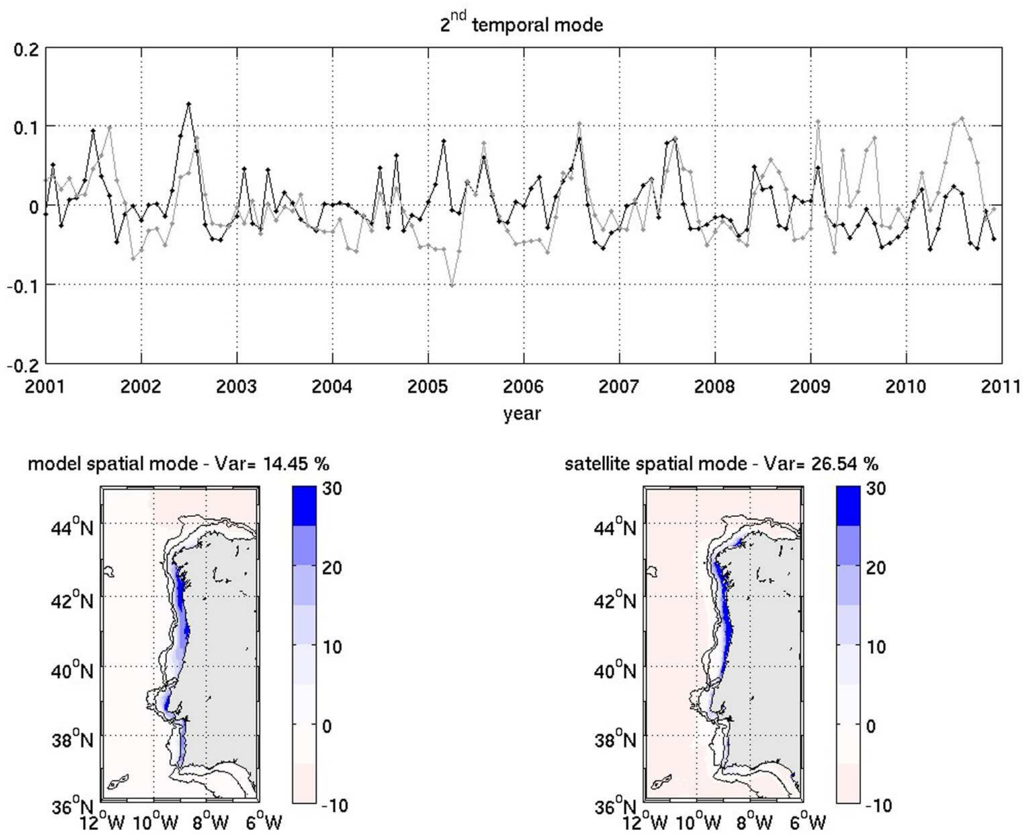

Figure 6: As for Fig. 5 but for the second mode of the EOF analysis.

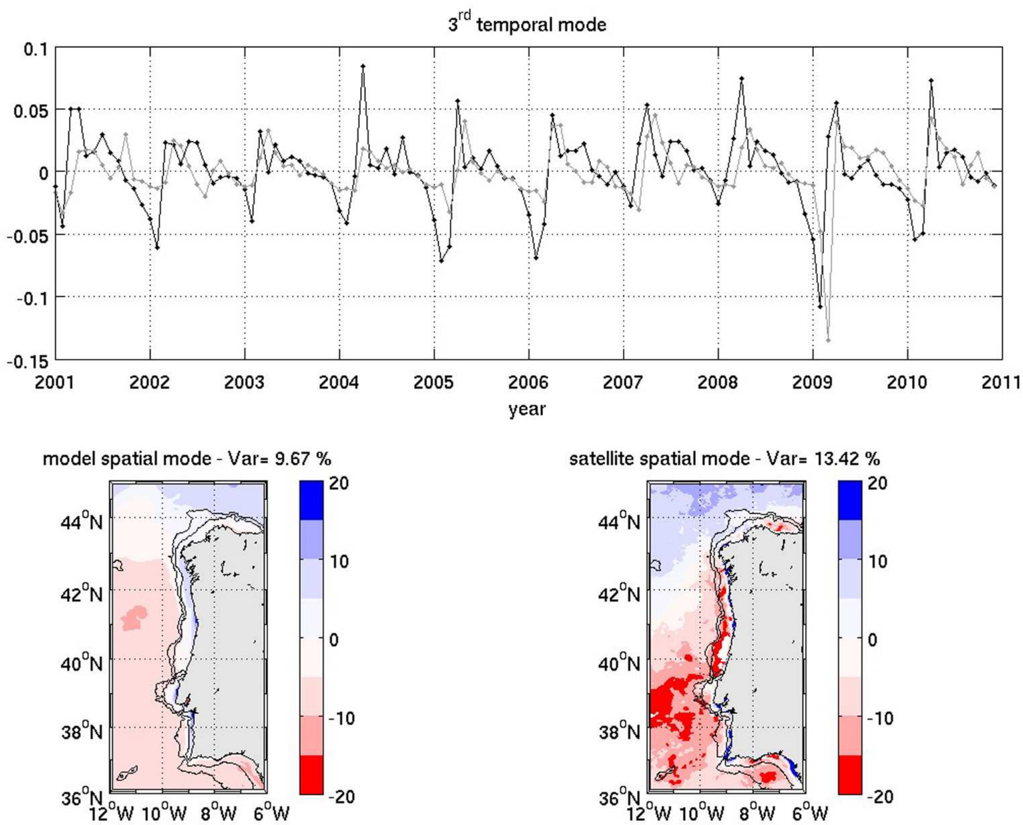

Figure 7: As for Fig. 5 but for the third mode of the EOF analysis.

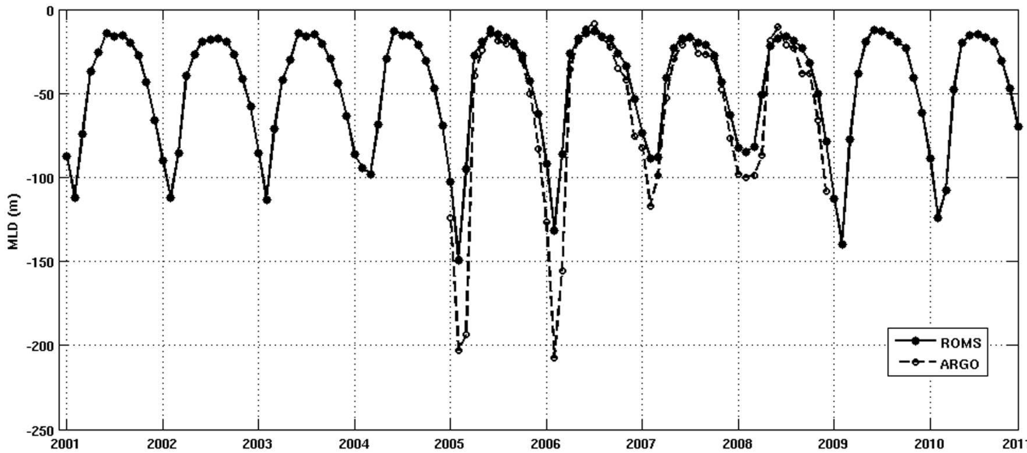

Figure 8: Monthly time series of ROMS domain averaged mixed layer depth (m) for the period 2001-2010 (solid line) and average mixed layer depth obtained from Argo floats data available for the same area (n>200 for every year) for the period 2005-2008 (dashed line) (Holte et al., 2010).

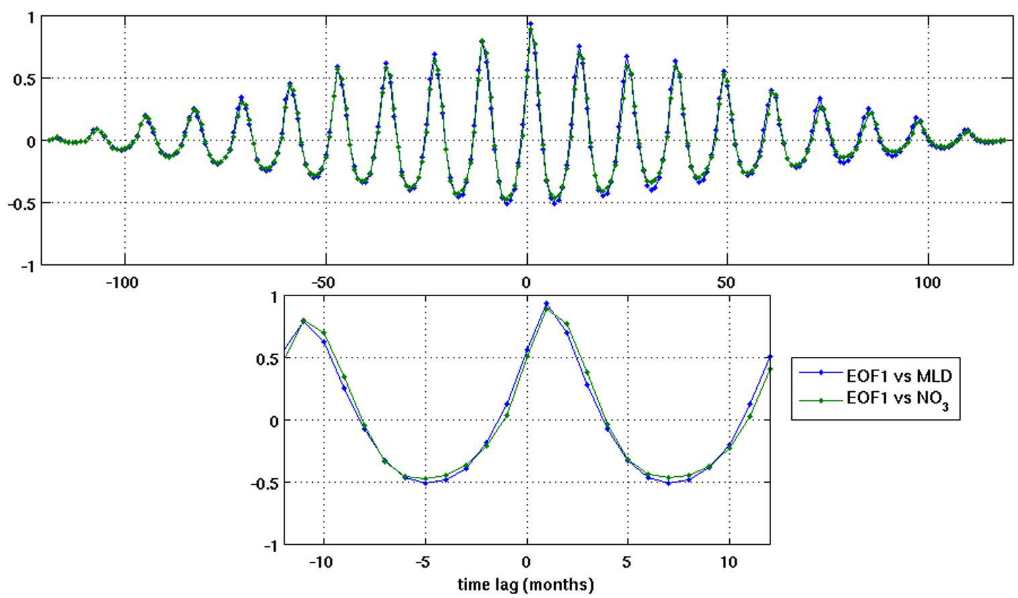

Figure 9: Cross-correlation between the *spring EOF* time series and the monthly mixed layer depth and the monthly NO_3. Upper panel: cross-correlation for the 10 years time series. Lower panel: zoom showing cross-correlation out to 12 months.

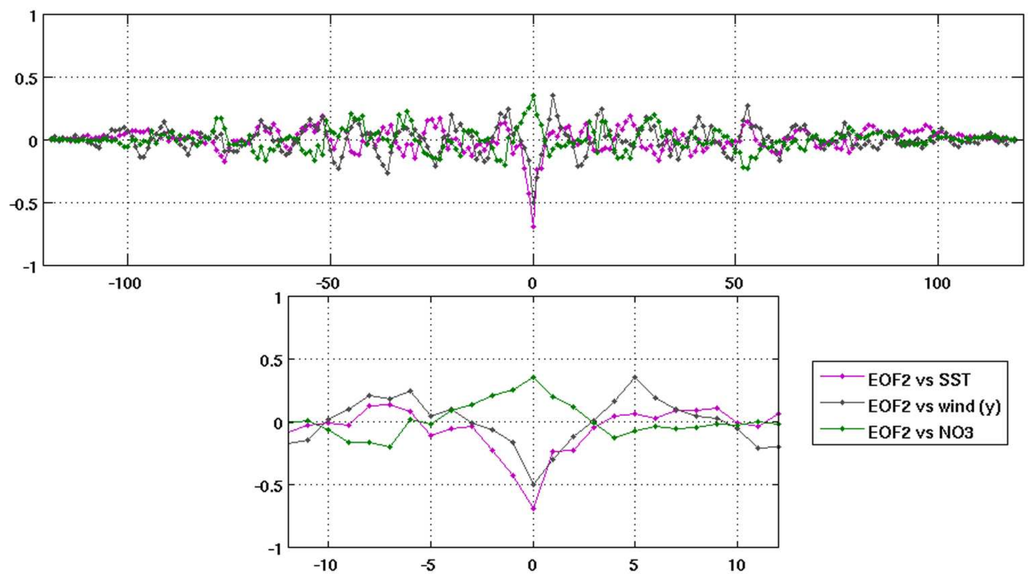

Figure 10: Cross-correlation between the *upwelling EOF* time series and: (1) the monthly SST at the shelf (40.5° N 9.5° W), after subtracting the seasonal cycle; (2) the monthly meridional component of the wind at the shelf (40.5° N 9.5° W); and (3) the monthly NO_3 after subtracting the seasonal cycle. Upper panel: cross-correlation for the 10 years time series. Lower panel: zoom showing cross-correlation out to 12 months.

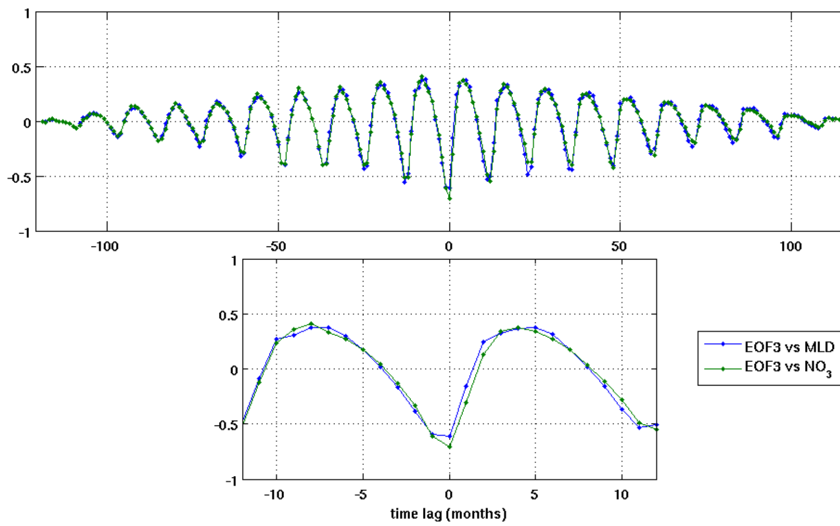

Figure 11: Cross-correlation between the *winter EOF* time series and: (1) the monthly mixed layer depth; (2) the monthly river Douro outflow; and the monthly NO_3. Upper panel: cross-correlation for the 10 years time series. Lower panel: zoom showing cross-correlation out to 12 months.

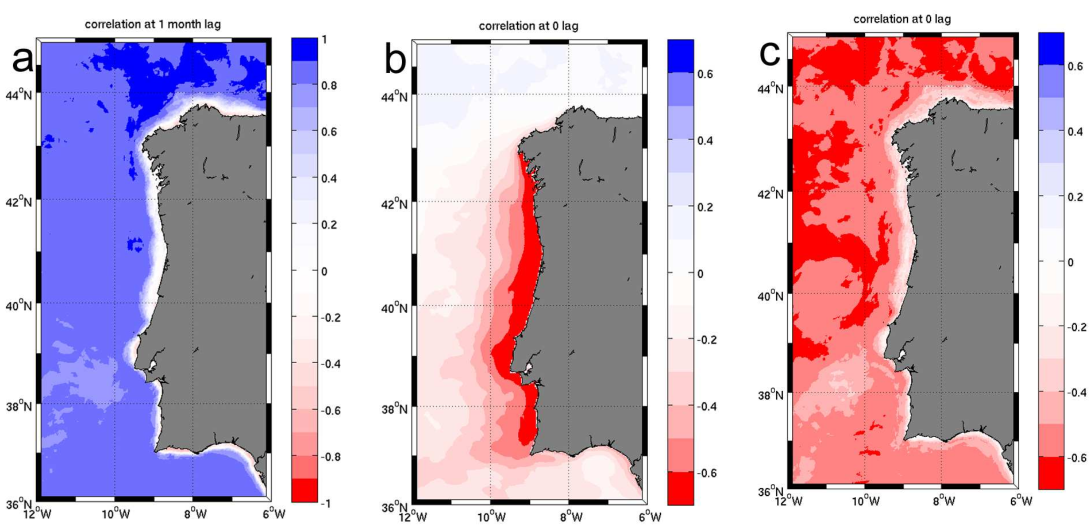

Figure 12: Map of correlation coefficients between: (a) *spring EOF* and MLD at 1 month lag; (b) *upwelling EOF* and SST at the shelf (40.5° N 9.5° W), after subtracting the seasonal variation, at 0 lag; (c) *winter EOF* and MLD at 0 lag.

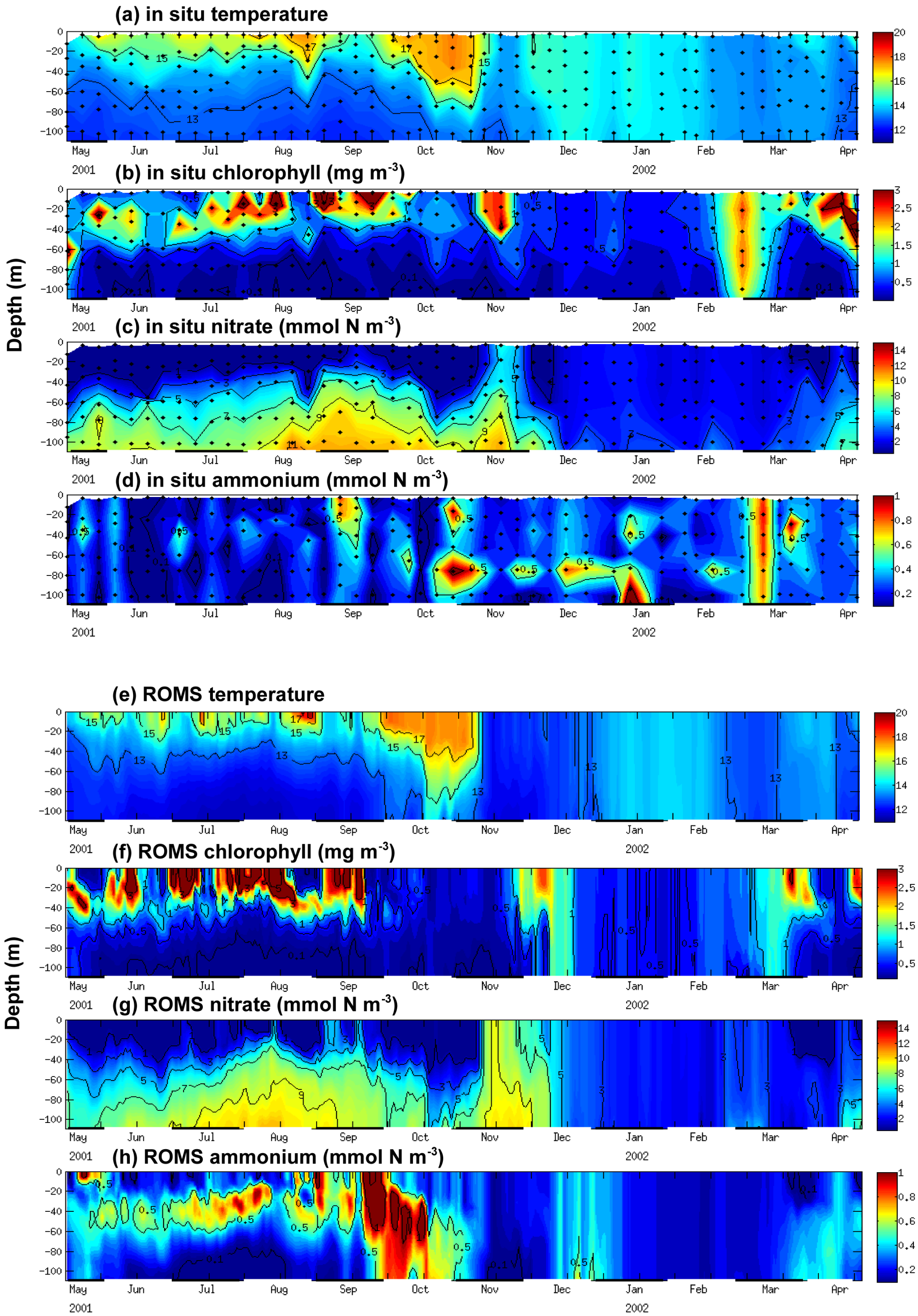

Figure 13: Hydrographic/biogeochemical data observed at a sampled station in NW Iberia (Fig. 1) between May 2001-April 2002 (a, b, c, d) compared with model outputs for the same period (e, f, g, h).

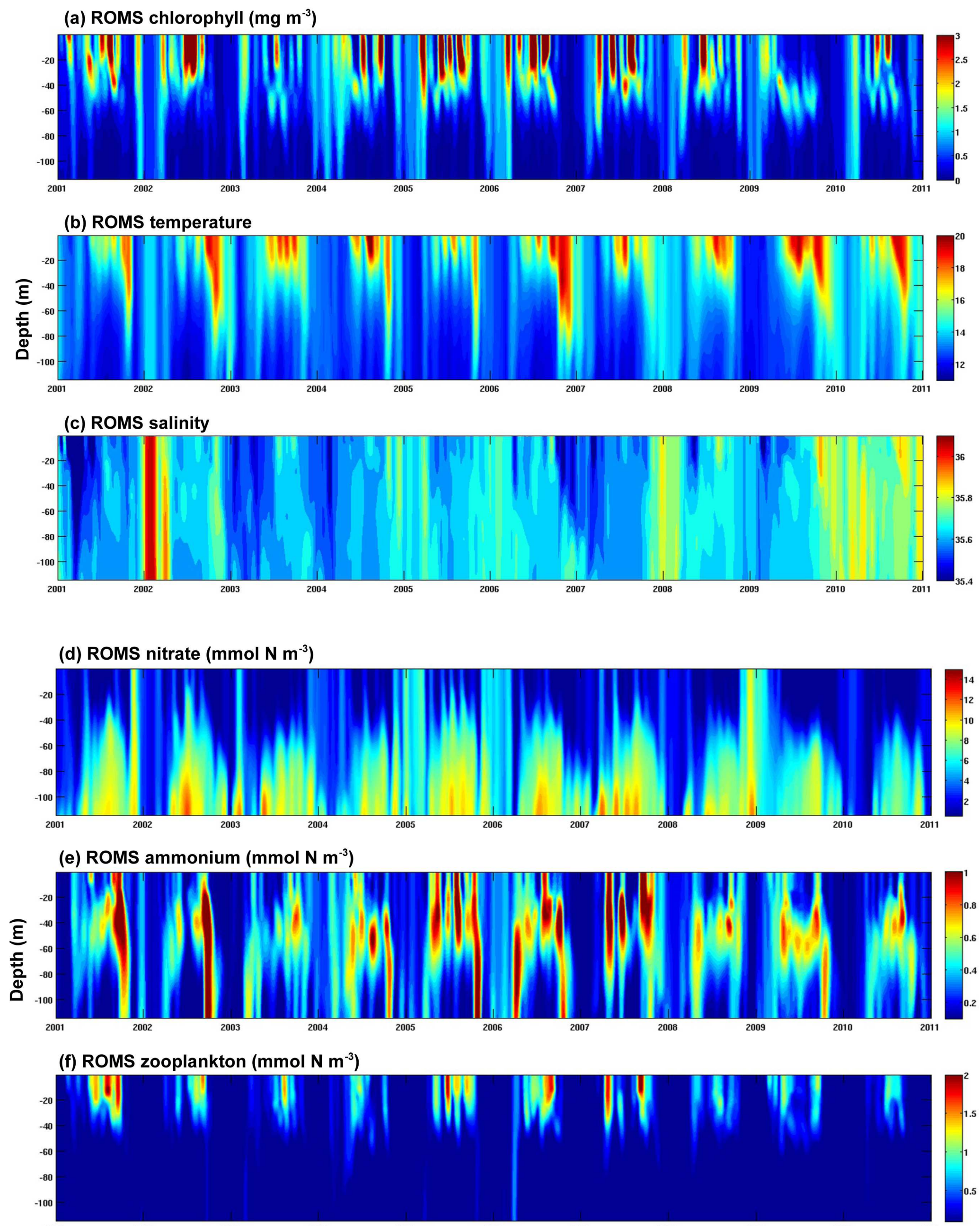

Figure 14: Interannual (2001-2010) model results (30-days running mean) for hydrography (temperature and salinity) and biogeochemistry (chlorophyll, zooplankton, nitrate and ammonium) at the same location of the DYBAGA station (Fig. 1).

Figure3a

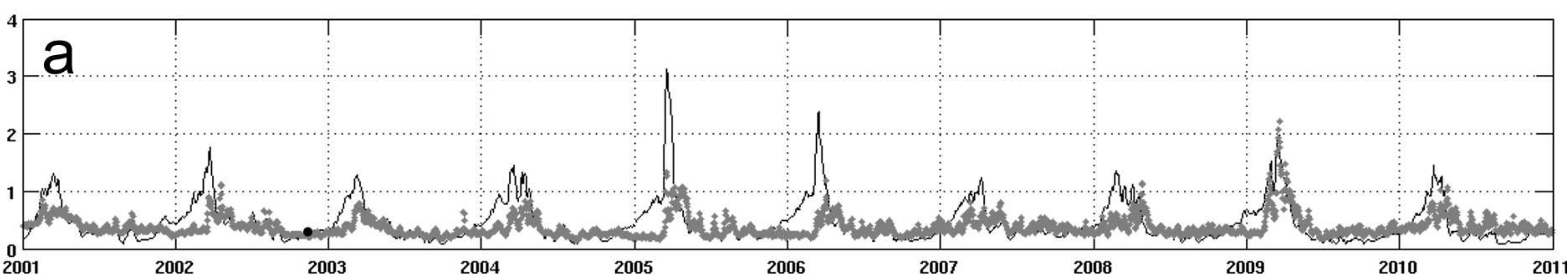
a
4
3
2
1
0
2001
2002
2003
2004
2005
2006
2007
2008
2009
2010
2011

Figure3b

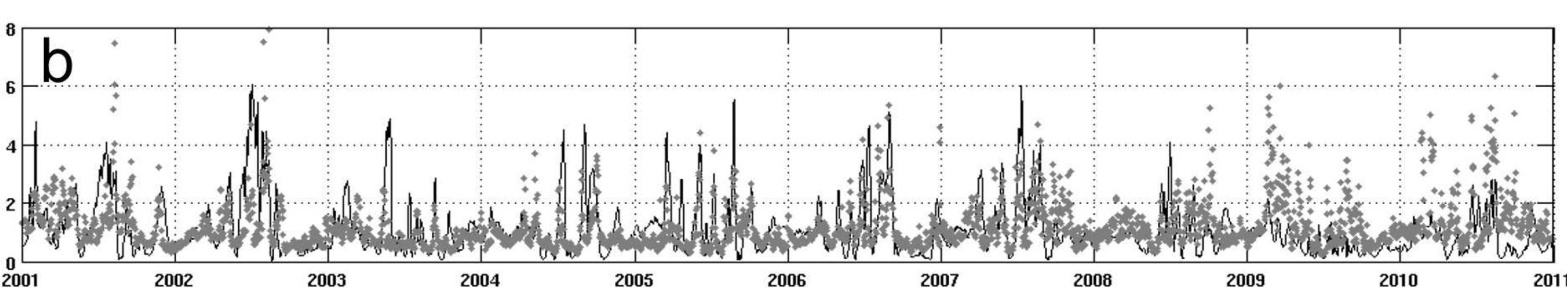
b
8
6
4
2
0
2001
2002
2003
2004
2005
2006
2007
2008
2009
2010
2011

Figure3c

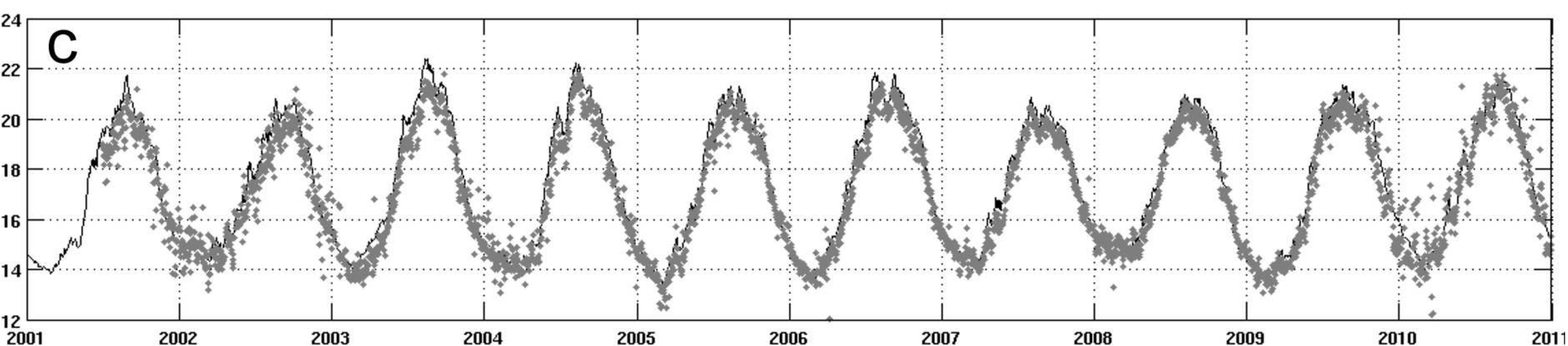
C
24
22
20
18
16
14
12
2001
2002
2003
2004
2005
2006
2007
2008
2009
2010
2011

Figure3d

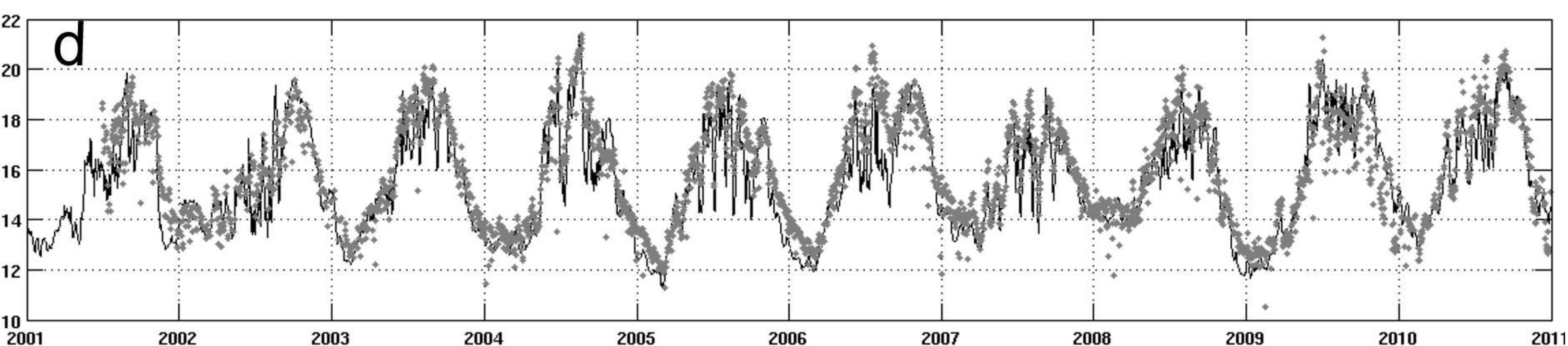
d
22
20
18
16
14
12
10
2001
2002
2003
2004
2005
2006
2007
2008
2009
2010
2011

Figure4

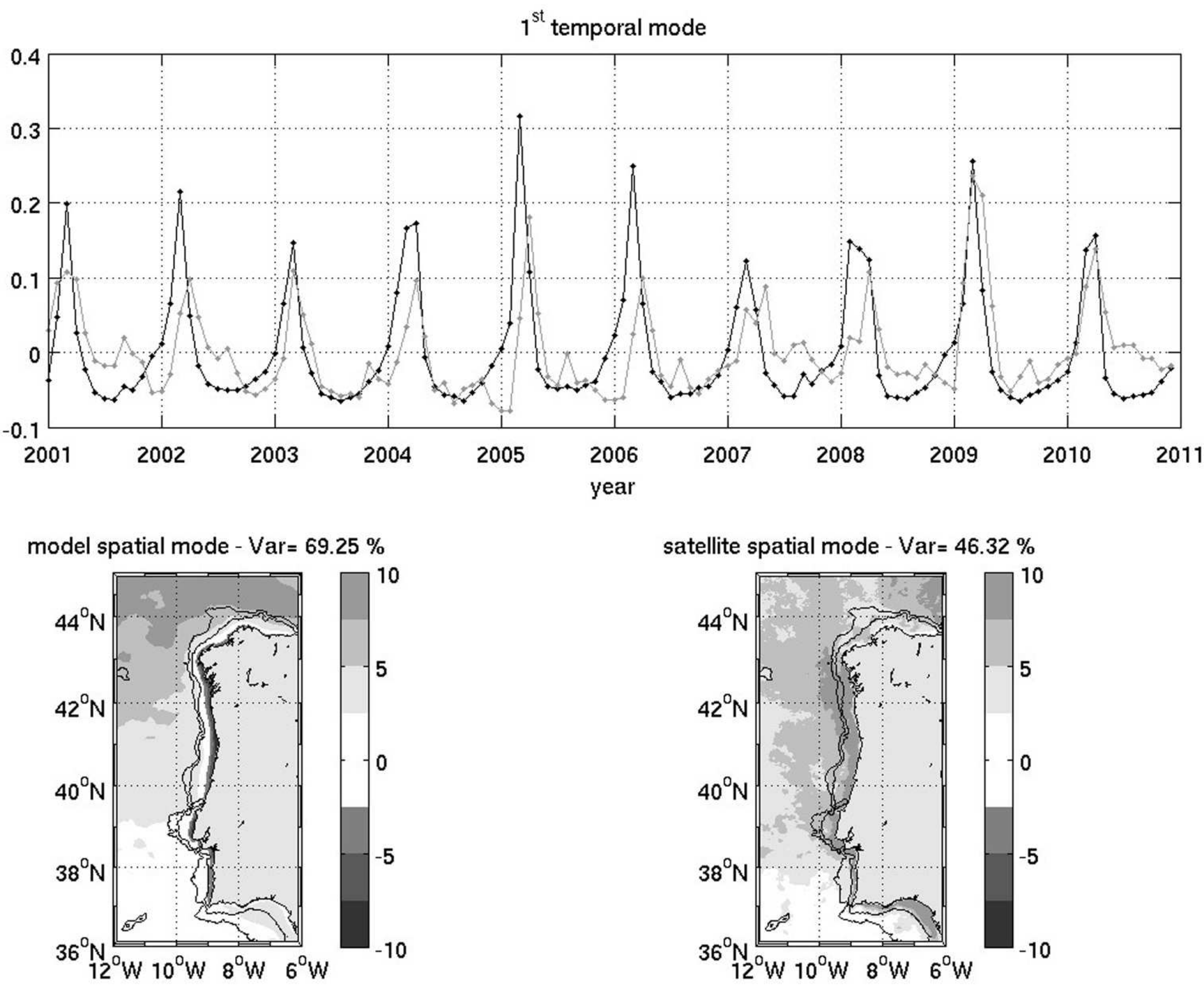

1st temporal mode
0.4
0.3
0.2
0.1
0
-0.1
2001
2002
2003
2004
2005
2006
2007
2008
2009
2010
2011
year
model spatial mode - Var= 69.25 %
satellite spatial mode - Var= 46.32 %
44°N
42°N
40°N
38°N
36°N
12°W
10°W
8°W
6°W
10
5
0
-5
-10

Figure5

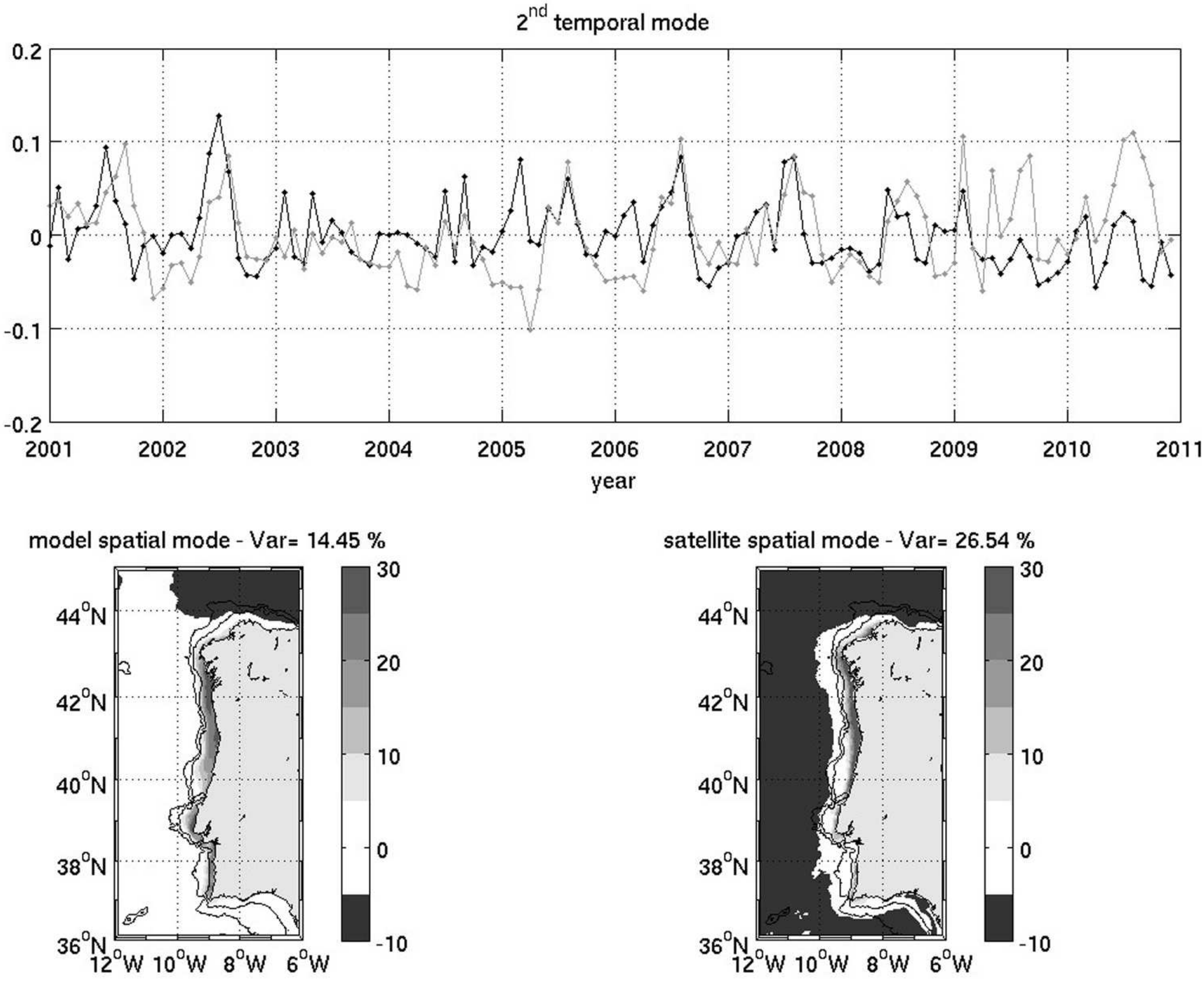
2nd temporal mode
0.2
0.1
0
-0.1
-0.2
2001
2002
2003
2004
2005
2006
2007
2008
2009
2010
2011
year
model spatial mode - Var= 14.45 %
satellite spatial mode - Var= 26.54 %
44°N
42°N
40°N
38°N
36°N
12°W
10°W
8°W
6°W
30
20
10
0
-10

Figure6

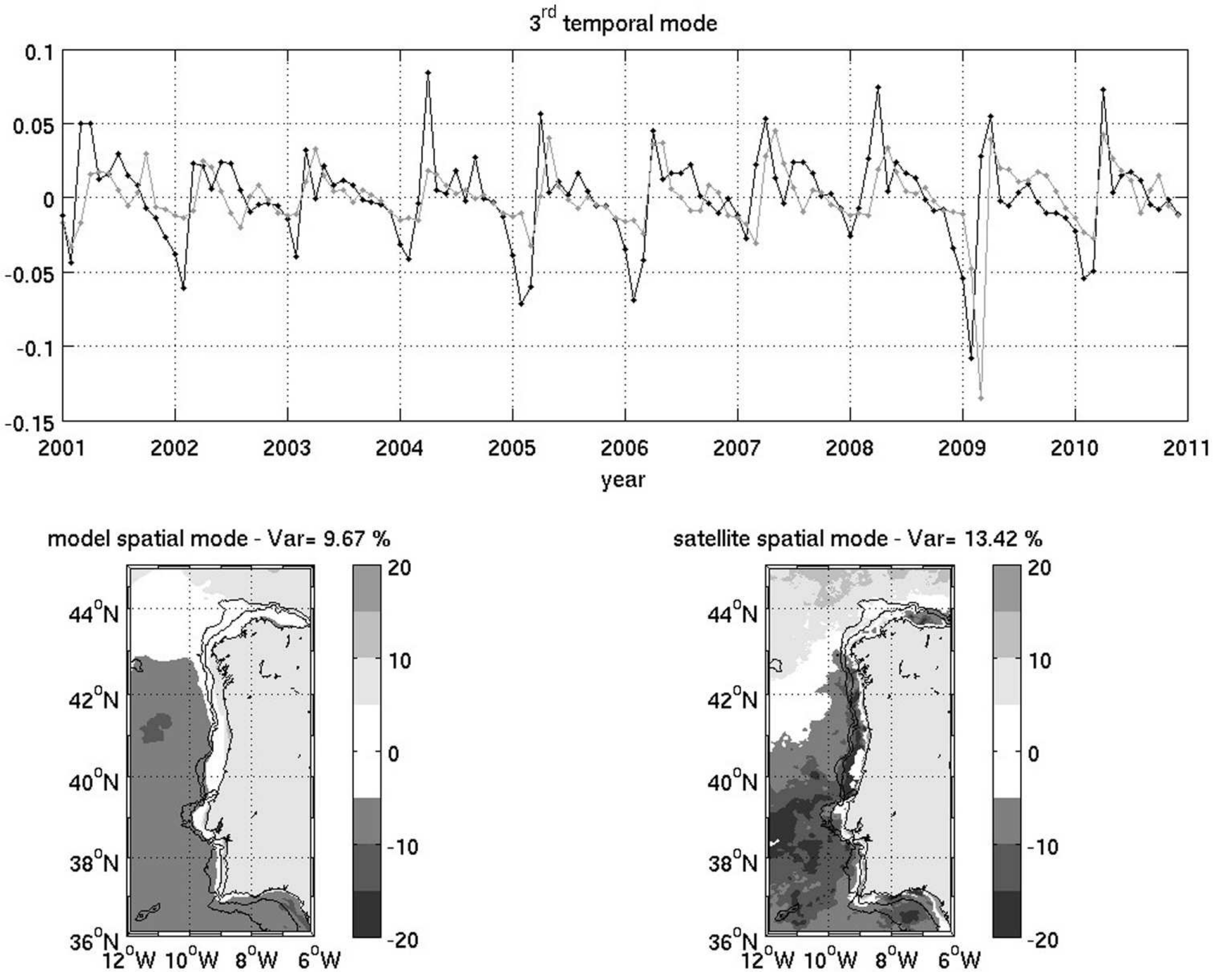

3rd temporal mode
0.1
0.05
0
-0.05
-0.1
-0.15
2001
2002
2003
2004
2005
2006
2007
2008
2009
2010
2011
year
model spatial mode - Var= 9.67 %
satellite spatial mode - Var= 13.42 %
44°N
42°N
40°N
38°N
36°N
12°W 10°W 8°W 6°W
20
10
0
-10
-20

Figure7a

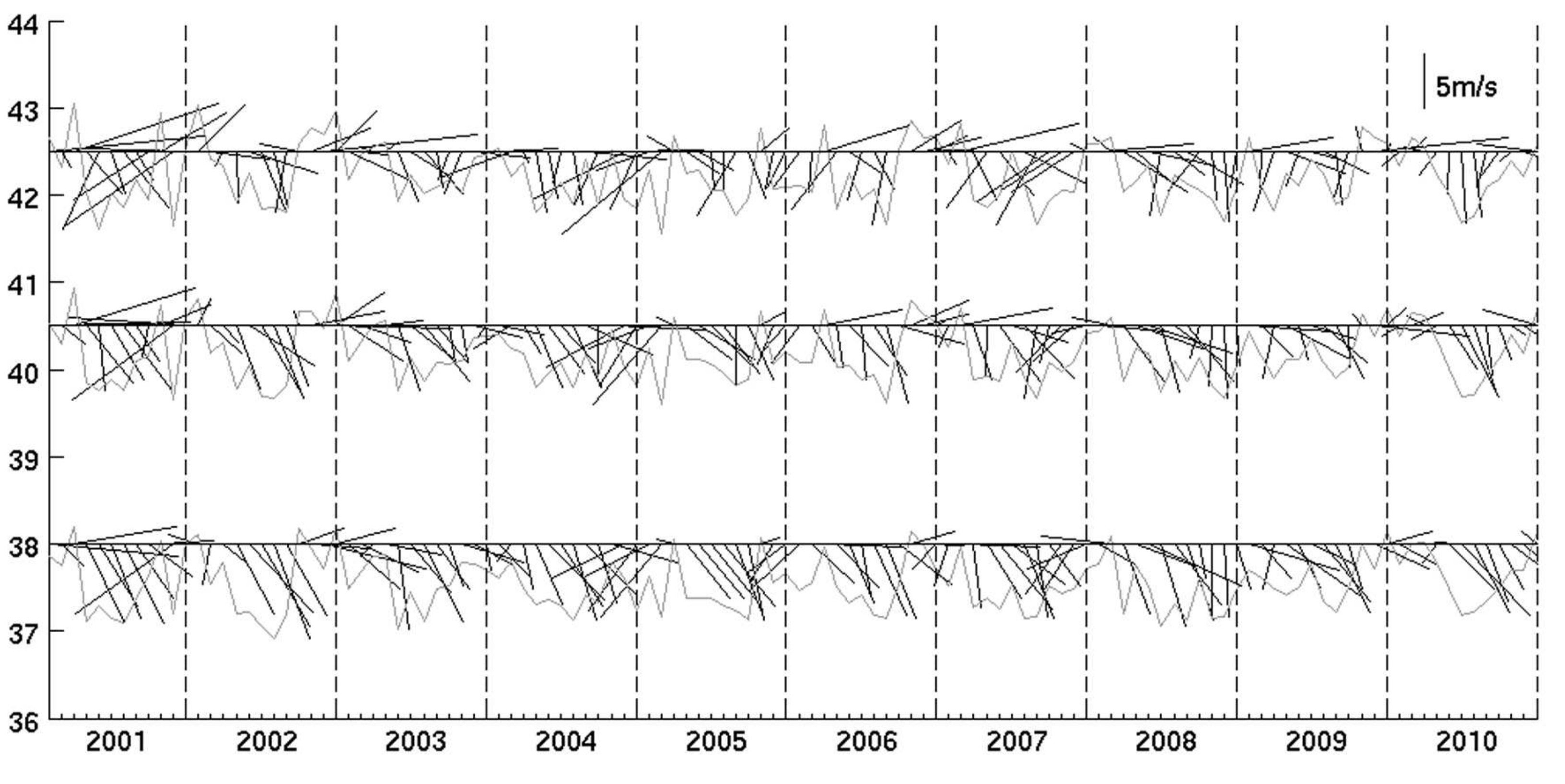

44
43
42
41
40
39
38
37
36
5m/s
2001
2002
2003
2004
2005
2006
2007
2008
2009
2010

Figure7b

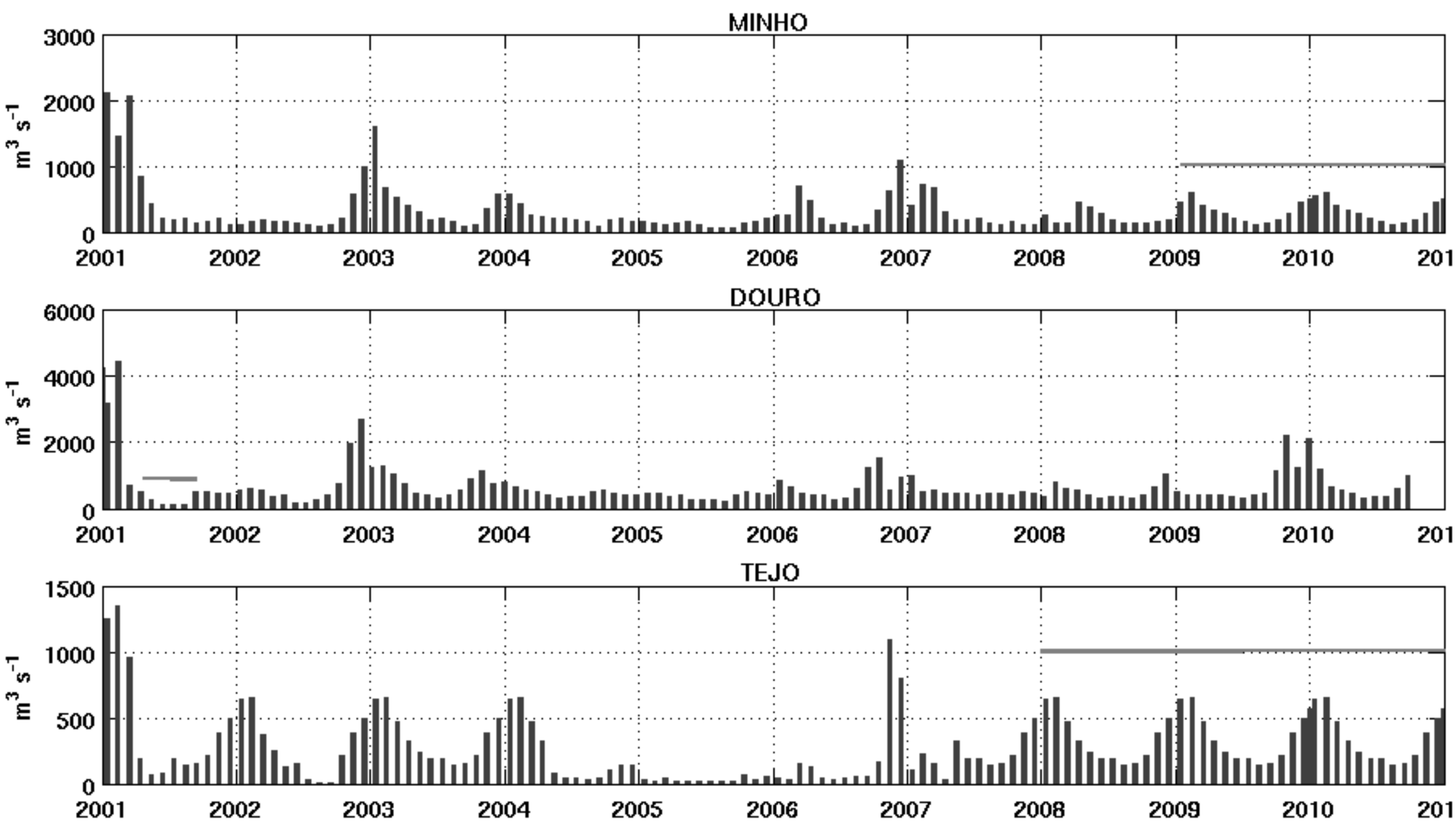
MINHO
3000
2000
1000
0
$m^3 s^{-1}$
2001
2002
2003
2004
2005
2006
2007
2008
2009
2010
2011
DOURO
6000
4000
2000
0
$m^3 s^{-1}$
2001
2002
2003
2004
2005
2006
2007
2008
2009
2010
2011
TEJO
1500
1000
500
0
$m^3 s^{-1}$
2001
2002
2003
2004
2005
2006
2007
2008
2009
2010
2011

Figure9a

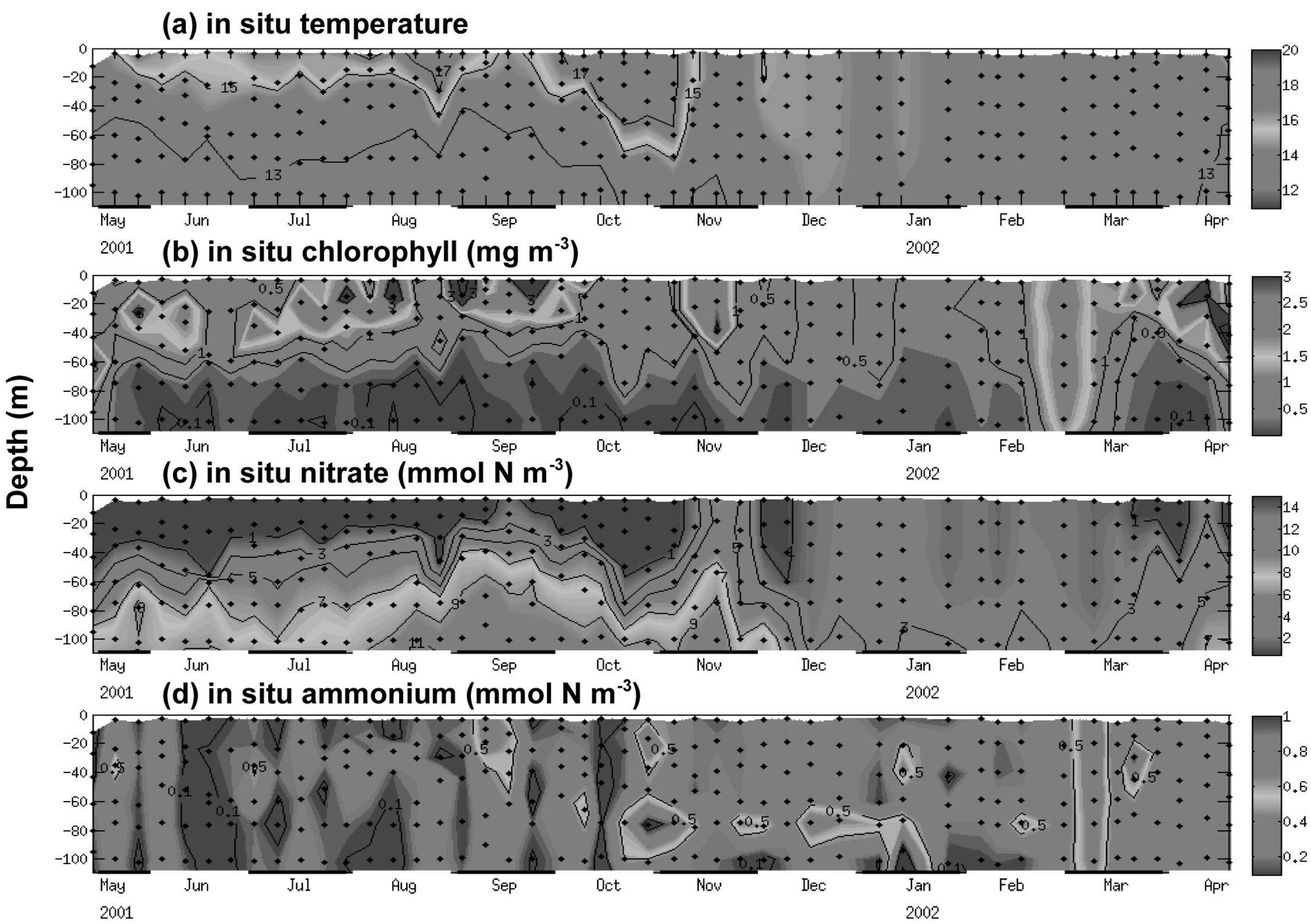

(a) in situ temperature
(b) in situ chlorophyll (mg m-3)
(c) in situ nitrate (mmol N m-3)
(d) in situ ammonium (mmol N m-3)
Depth (m)
May
Jun
Jul
Aug
Sep
Oct
Nov
Dec
Jan
Feb
Mar
Apr
2001
2002

Figure9b

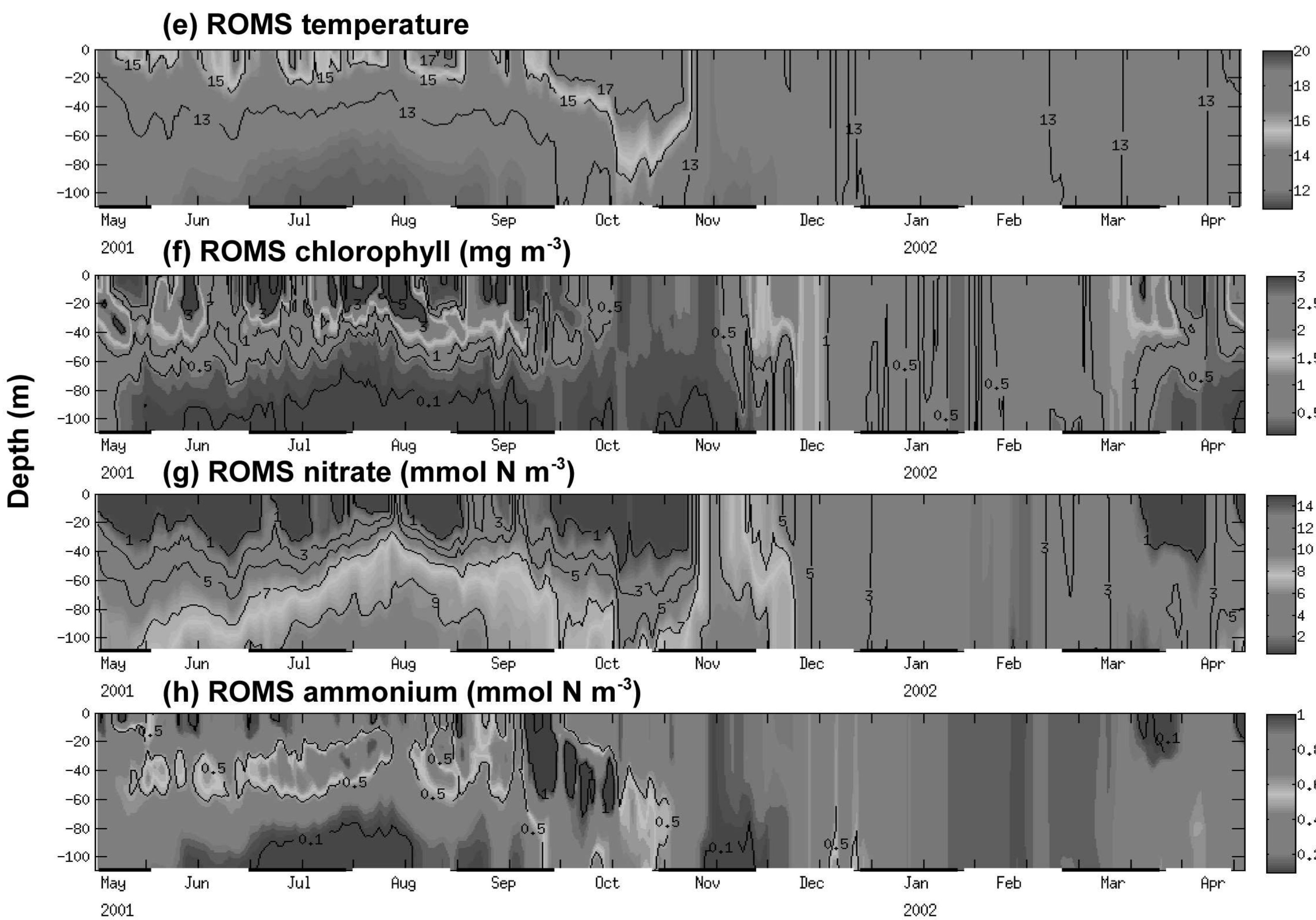
(e) ROMS temperature
(f) ROMS chlorophyll (mg m-3)
(g) ROMS nitrate (mmol N m-3)
(h) ROMS ammonium (mmol N m-3)
Depth (m)
May
Jun
Jul
Aug
Sep
Oct
Nov
Dec
Jan
Feb
Mar
Apr
2001
2002

Figure11

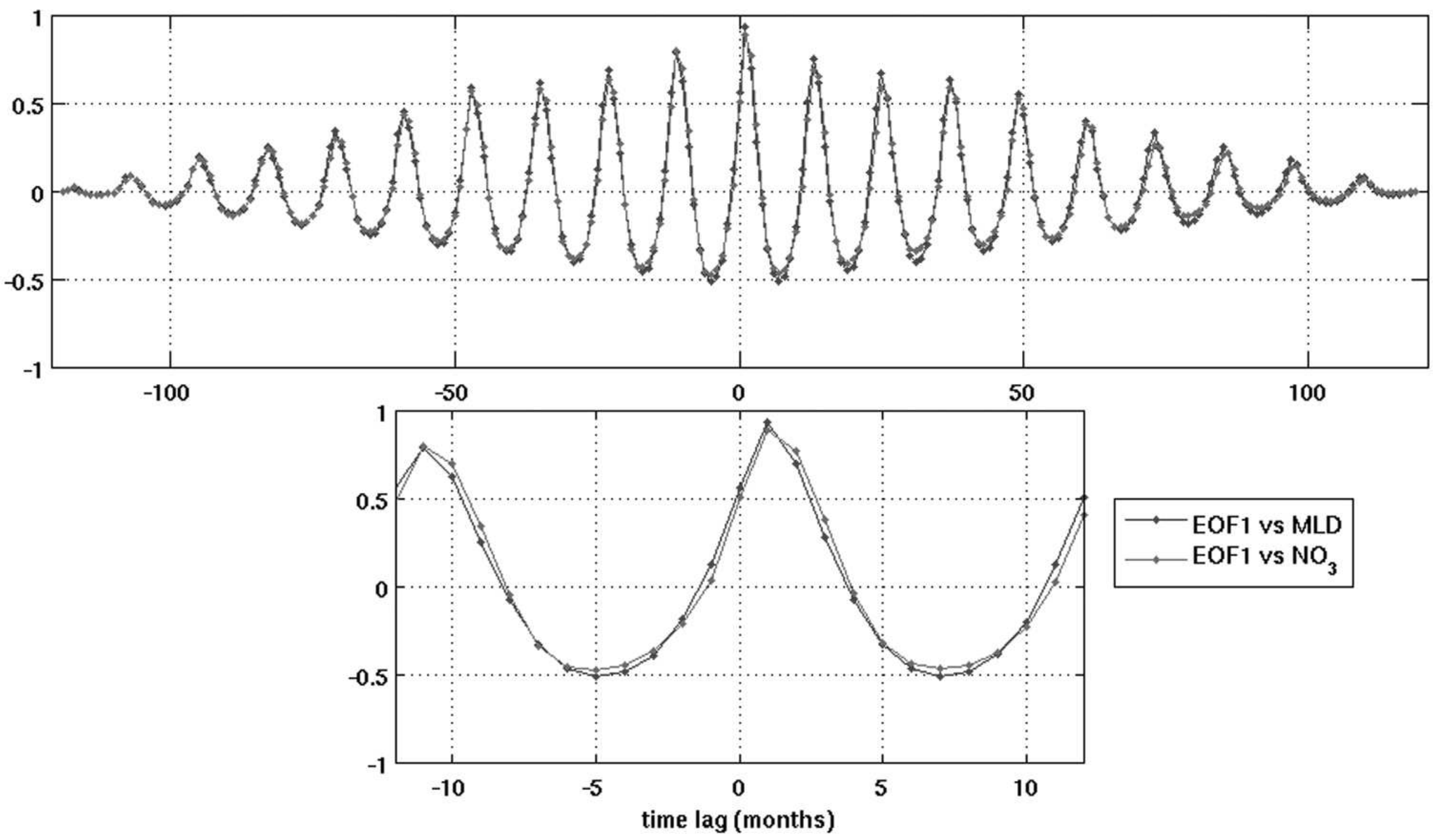

1
0.5
0
-0.5
-1
-100
-50
0
50
100
1
0.5
0
-0.5
-1
-10
-5
0
5
10
time lag (months)
EOF1 vs MLD
EOF1 vs NO_3

Figure12

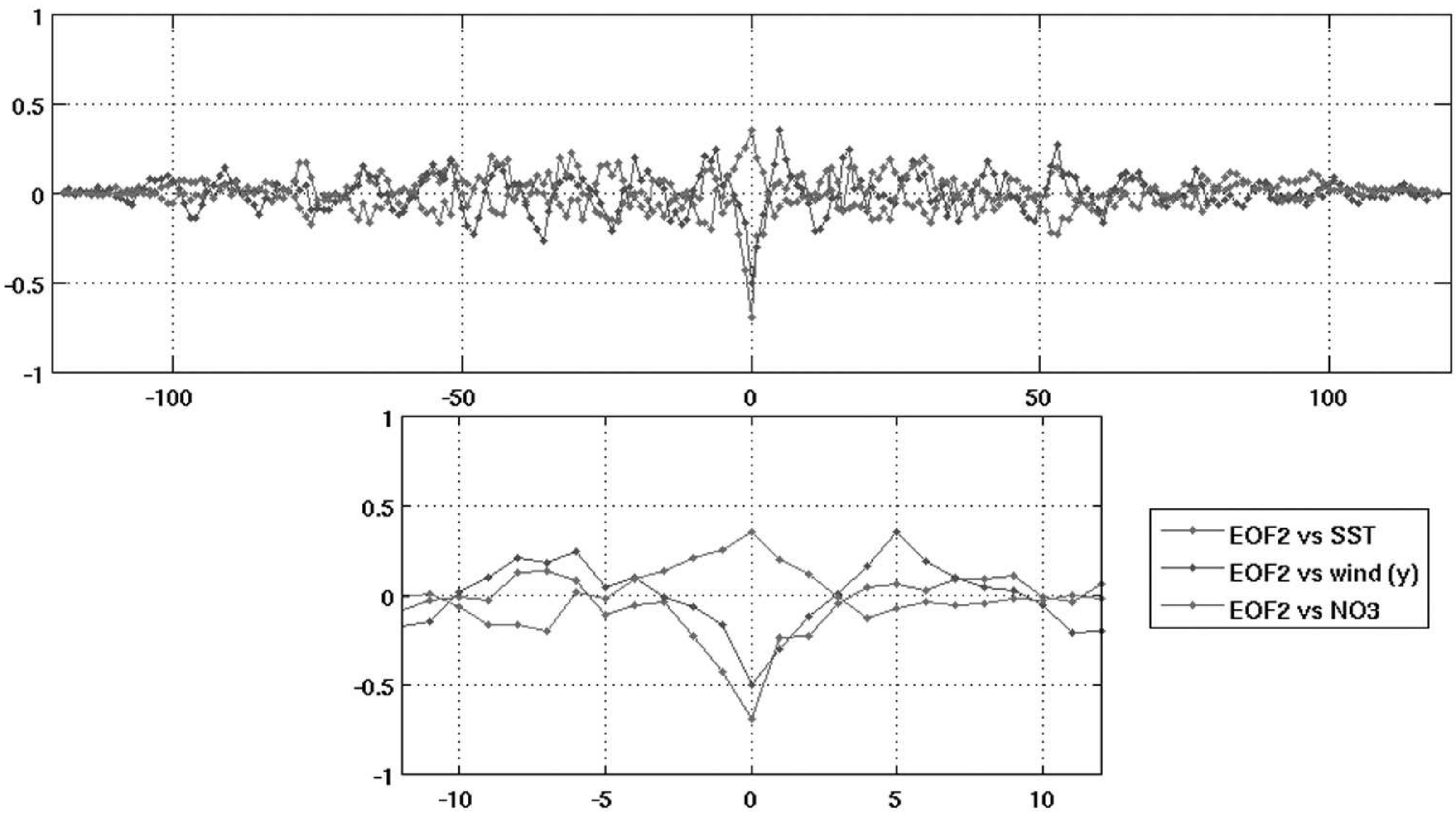
1
0.5
0
-0.5
-1
-100
-50
0
50
100
1
0.5
0
-0.5
-1
-10
-5
0
5
10
EOF2 vs SST
EOF2 vs wind (y)
EOF2 vs NO3

Figure13

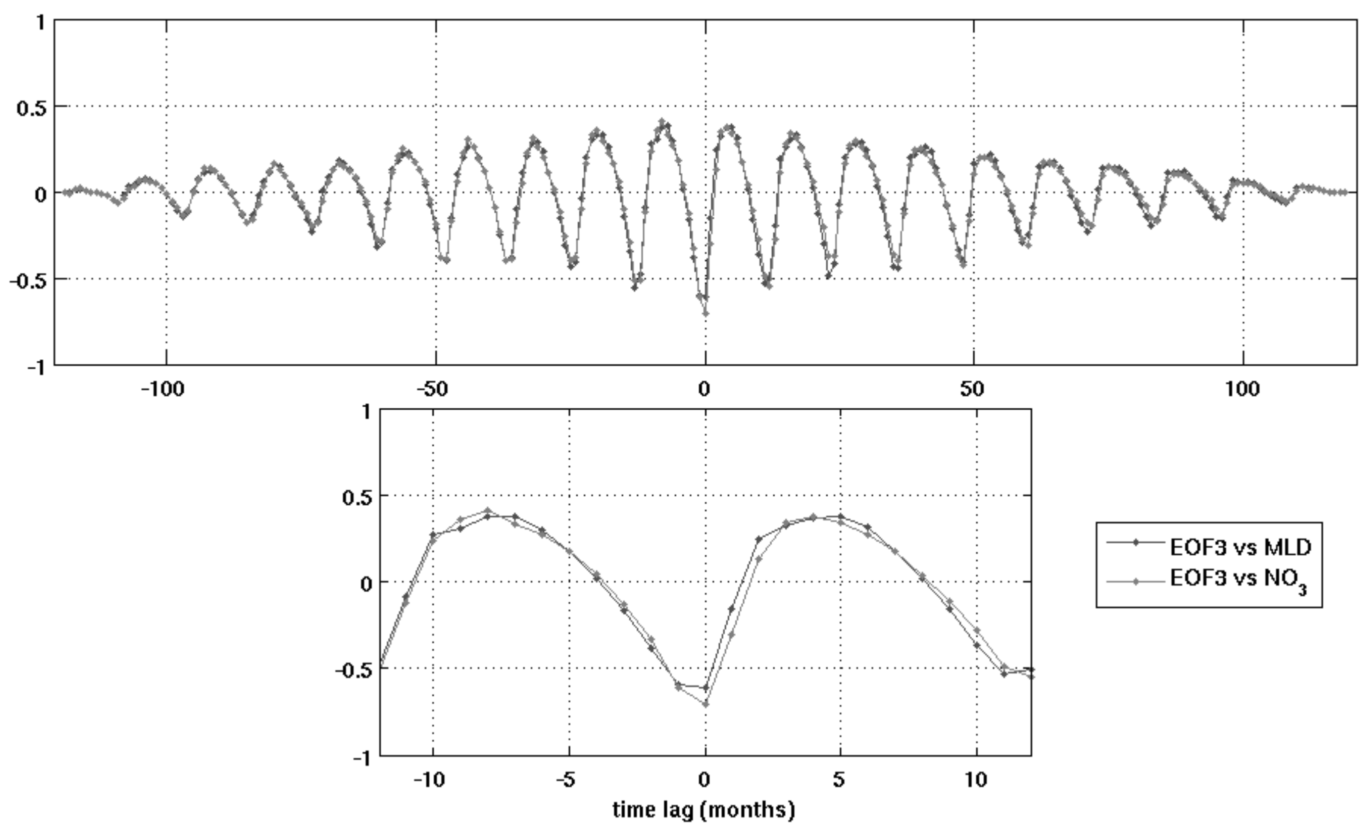

1
0.5
0
-0.5
-1
-100
-50
0
50
100
1
0.5
0
-0.5
-1
-10
-5
0
5
10
time lag (months)
EOF3 vs MLD
EOF3 vs NO_3

Figure14a

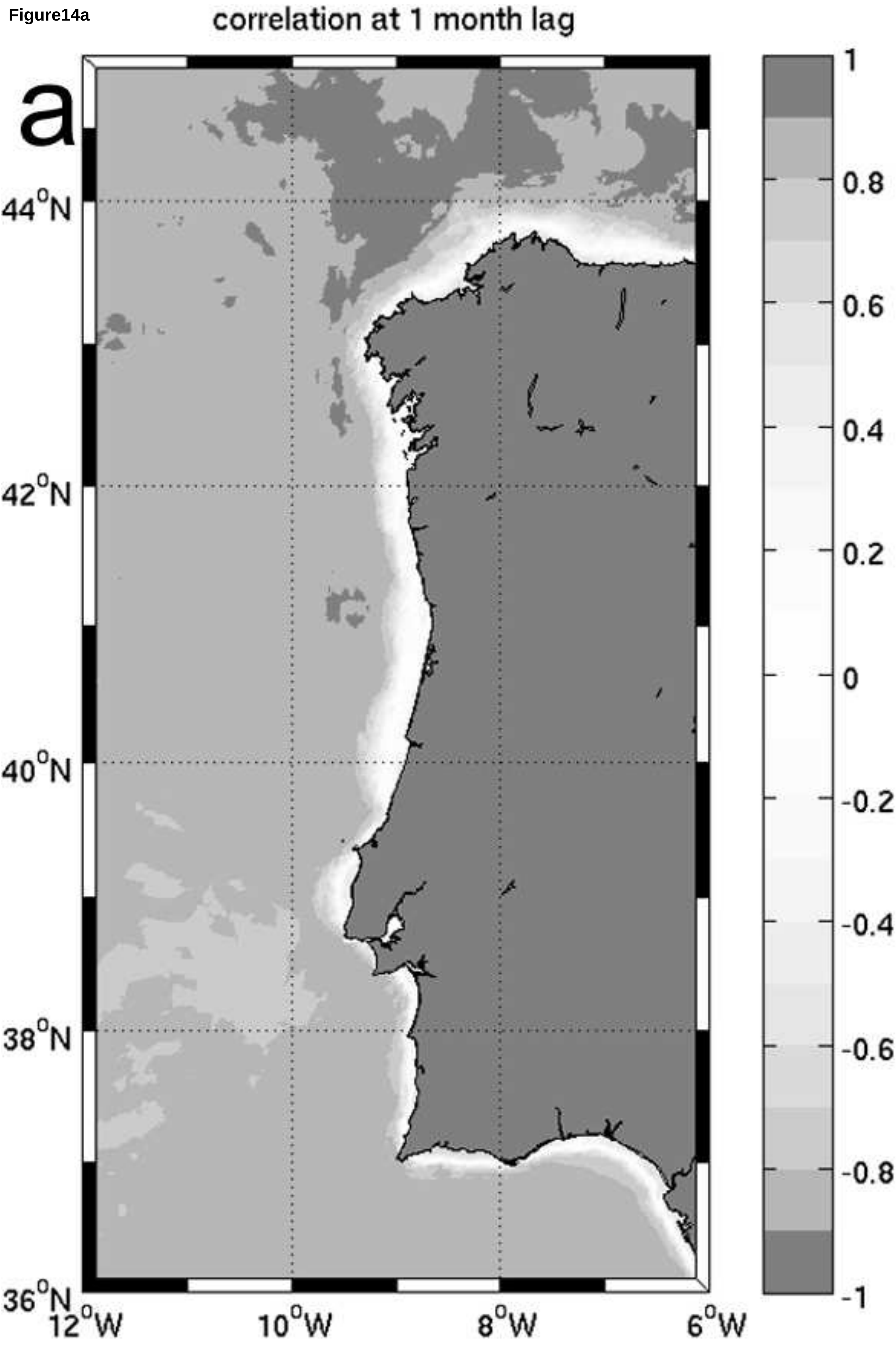
correlation at 1 month lag
a
44°N
42°N
40°N
38°N
36°N
12°W
10°W
8°W
6°W
1
0.8
0.6
0.4
0.2
0
-0.2
-0.4
-0.6
-0.8
-1

Figure14b

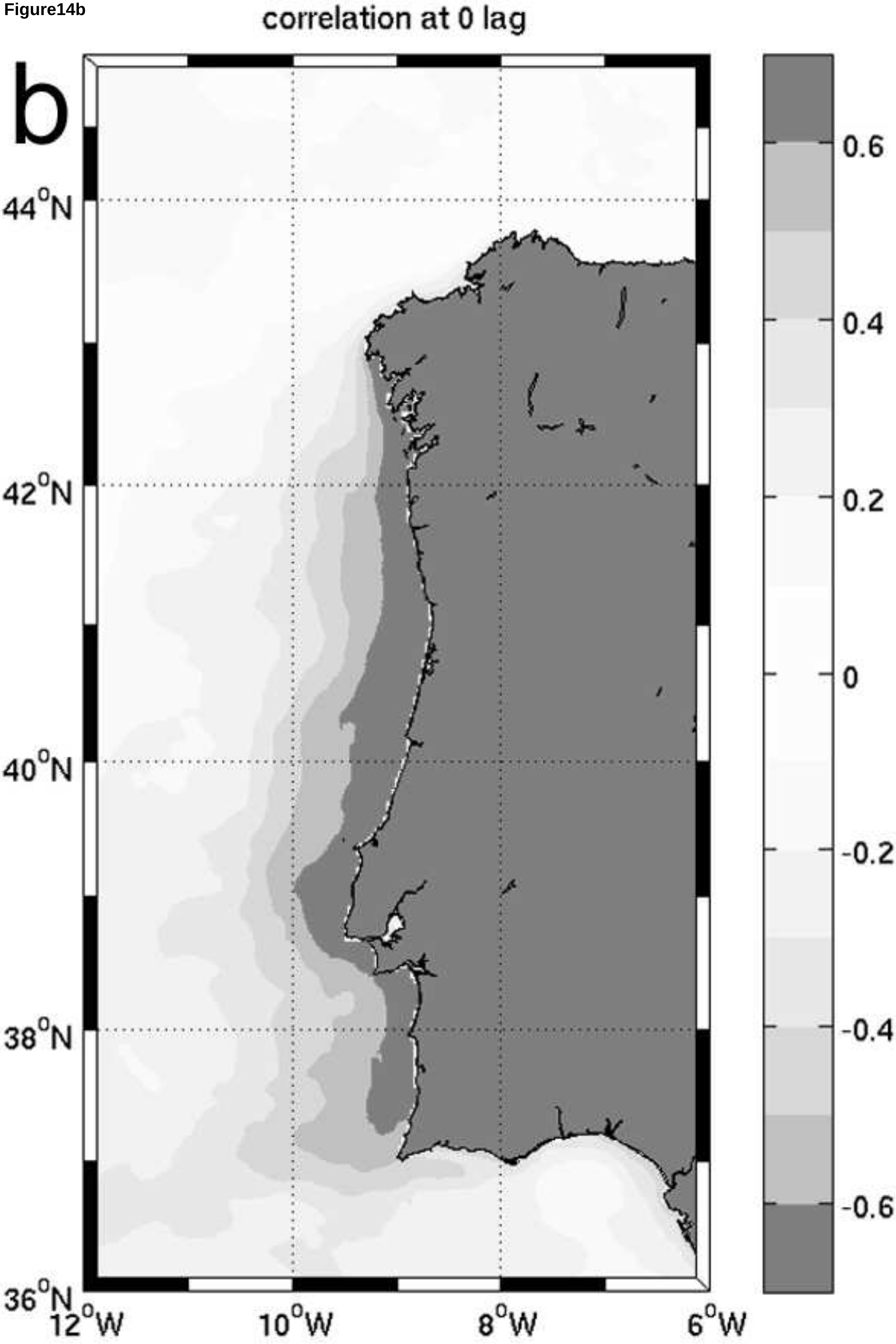

correlation at 0 lag
b
44⁰N
42⁰N
40⁰N
38⁰N
36⁰N
12⁰W
10⁰W
8⁰W
6⁰W
0.6
0.4
0.2
0
-0.2
-0.4
-0.6

Figure14c

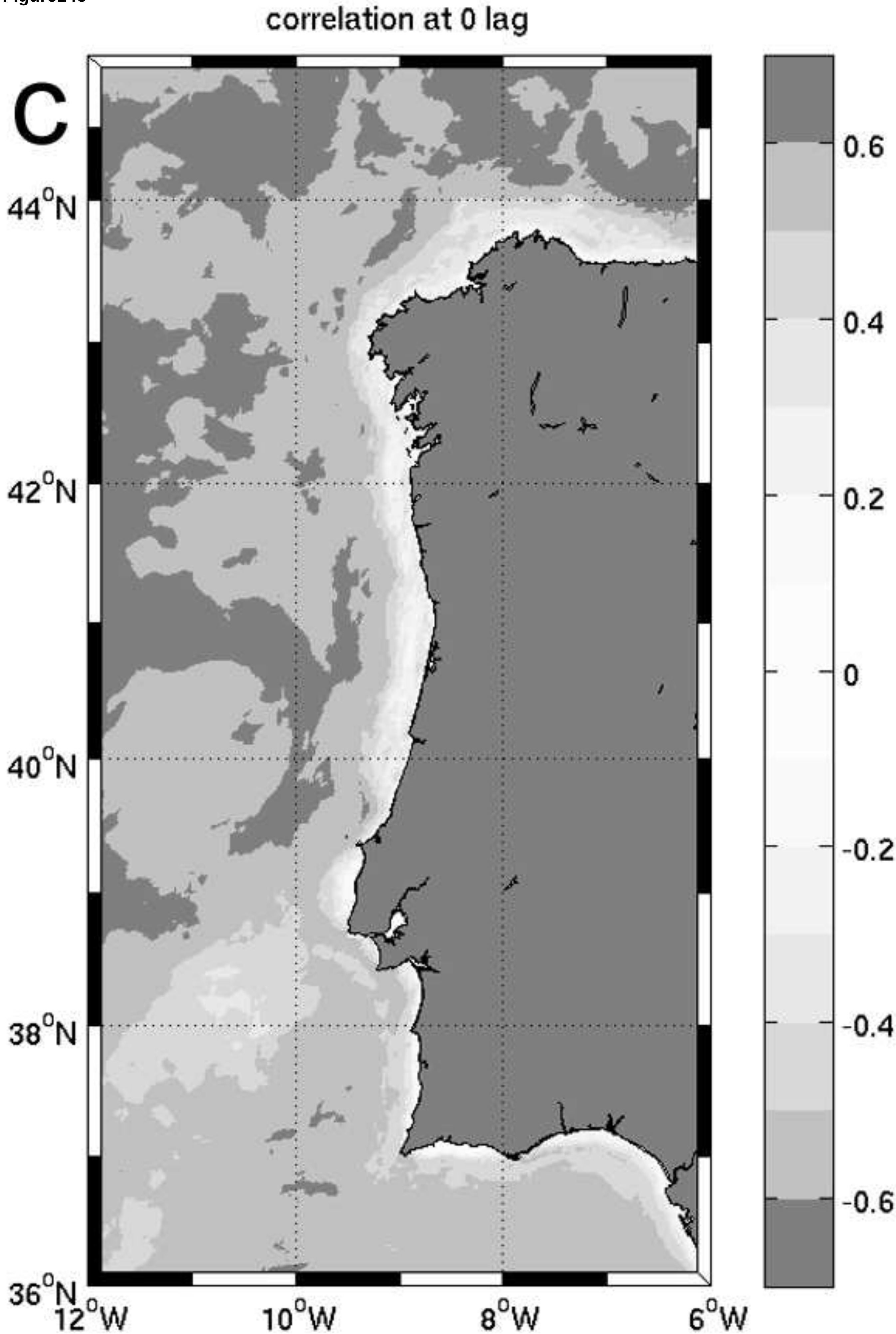

correlation at 0 lag
C
44°N
42°N
40°N
38°N
36°N
12°W
10°W
8°W
6°W
0.6
0.4
0.2
0
-0.2
-0.4
-0.6